AD-A130 757 A STUDY OF THE AERODYNAMIC INTERACTIONS OF THE TAIL ROTOR AND FIN(U) BOEING VERTOL CO PHILADELPHIA PA P F SHERIDAN ET AL. 06 JUN 83 ARO-15710.2-EG 1/1

UNCLASSIFIED DAAG29-78-C-0021 F/G 20/4 NL

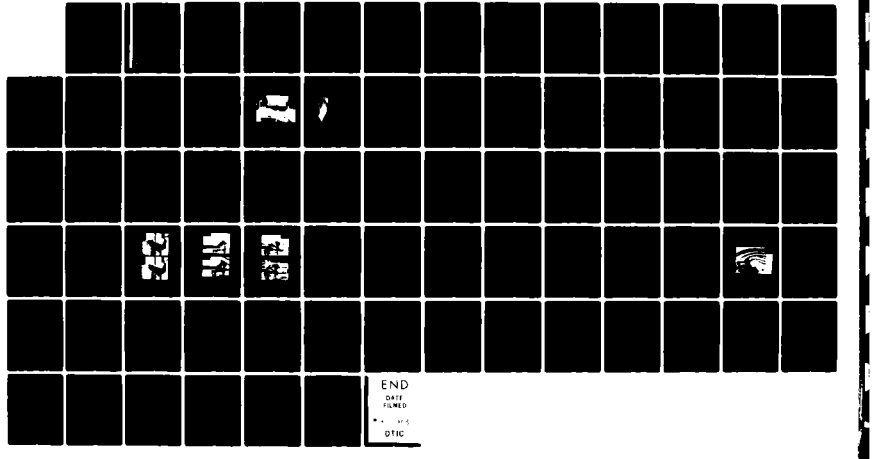

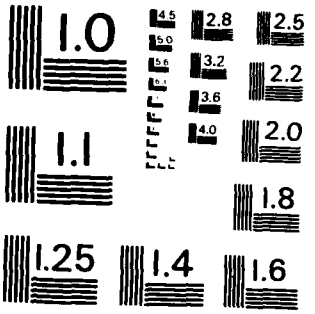

A Study of the Aerodynamic Interactions of the Tail Rotor and Fin

FINAL REPORT

P. F. Sheridan
E. J. Hanker, Jr.
B. B. Blake

June 6, 1983

U.S. Army Research Office
Contract DAAG29-78-C-0021

BOEING VERTOL COMPANY
P.O. Box 16858
Philadelphia, Pennsylvania 19142

SECURITY CLASSIFICATION OF THIS PAGE (When Data Entered)

REPORT DOCUMENTATION PAGE

READ INSTRUCTIONS BEFORE COMPLETING FORM

1. REPORT NUMBER	2. GOVT ACCESSION NO. AD-A130757 / 3. RECIPIENT'S CATALOG NUMBER
4. TITLE (and Subtitle) A Study of the Aerodynamic Interactions of the Tail Rotor and Fin	5. TYPE OF REPORT & PERIOD COVERED Final Report 17 July 1978 - 1 Feb. 1983 / 6. PERFORMING ORG. REPORT NUMBER
7. AUTHOR(s) Philip F. Sheridan, Edward J. Hanker, Jr., Bruce B. Blake	8. CONTRACT OR GRANT NUMBER(s) Contract DAAG29-78-C-0021
9. PERFORMING ORGANIZATION NAME AND ADDRESS Boeing Vertol Company, P.O. Box 16858, Philadelphia, Pennsylvania 19142	10. PROGRAM ELEMENT, PROJECT, TASK AREA & WORK UNIT NUMBERS N/A
11. CONTROLLING OFFICE NAME AND ADDRESS U.S. Army Research Office, Post Office Box 12211, Research Triangle Park, N.C. 27709	12. REPORT DATE May 31, 1983 / 13. NUMBER OF PAGES 73
14. MONITORING AGENCY NAME & ADDRESS(if different from Controlling Office)	15. SECURITY CLASS. (of this report) Unclassified / 15a. DECLASSIFICATION/DOWNGRADING SCHEDULE

16. DISTRIBUTION STATEMENT (of this Report)

Approved for public release; distribution unlimited

17. DISTRIBUTION STATEMENT (of the abstract entered in Block 20, if different from Report)

NA

18. SUPPLEMENTARY NOTES

The view, opinions, and/or findings contained in this report are those of the author(s) and should not be construed as an official Department of the Army position, policy, or decision, unless so designated by other documentation.

19. KEY WORDS (Continue on reverse side if necessary and identify by block number)

Aerodynamic Interaction	Ground Effect	Nap-of-the-Earth
Configuration Aerodynamics	Ground Vortex	Powered Model
Configuration	Helicopter	Rotor
Empennage	Interaction	Vortex
	Interference	Wind Tunnel

20. ABSTRACT (Continue on reverse side if necessary and identify by block number)

The results of a wind tunnel investigation of the aerodynamic interaction of the tail rotor and fin are presented. Model loads data were measured for a 1/4.85 scale model of the YUH-61A. Tests were conducted deep in ground effect at wind speeds ranging from 0 to 45 knots; representative of Nap-of-the-Earth. Flow visualization studies provided additional insight into the flow mechanisms at work such as the ground vortex. Distributional flow characteristics, particularly the location and structure of the main rotor tip vortex, were

DD FORM 1 JAN 73 1473 EDITION OF 1 NOV 65 IS OBSOLETE

Unclassified

SECURITY CLASSIFICATION OF THIS PAGE (When Data Entered)

20. (Continued)

measured by a hot film probe. A variable fin incidence mechanism was incorporated in the model to measure the integrated flow at the empennage. Adverse fin force and tail rotor power variations are measured as functions of airspeed, wind azimuth, tail rotor thrust and main rotor thrust.

FOREWORD

This final report presents the results of a wind tunnel investigation of the aerodynamic interaction of the tail rotor and fin of the single rotor helicopter configuration. A 1/4.85 scale model of the YUH-61A was tested in the Boeing Vertol V/STOL wind tunnel deep in ground effect where the aerodynamic environment is very complex due to the deflection of the main rotor wake. Model forces and moments were measured as a function of airspeed, wind azimuth, tail rotor thrust and main rotor thrust. Wind speeds were varied from 0 to 45 knots to represent the Nap-of-the-Earth (NOE) flight regime. A summary of the significant findings from the recent wind tunnel test is presented in this report.

The wind tunnel investigation was funded jointly by the Army Research Office and the Applied Technology Laboratory from Ft. Eustis, Virginia. The ATL contract was entitled "Investigation of Operational and Design Factors Resulting from Main Rotor and Tail Rotor Interactions" and carried the number DAAK51-80-C-0025. Mr. Robert P. Smith, from the Aeromechanics Technical Area at ATL was the technical monitor for that contract.

This document is dedicated to the memory of Phil Sheridan. Phil, the original project engineer for this program, died suddenly immediately following the experimental phase of the contract. Phil dedicated many years of his life to the study of interactional aerodynamics beginning in the early seventies during the UTTAS program. During his career Phil had compiled a comprehensive data base pertaining to both the steady and unsteady effects of interactional aerodynamics. This data base will prove to be the foundation for the development of semi-empirical math models of these highly complex aerodynamic phenomena. Phil's expertise in this field will surely be missed.

TABLE OF CONTENTS

LIST OF ILLUSTRATIONS

LIST OF TABLES

NOMENCLATURE

A	rotor disk area, ft^2
$\overline{A}$	tail rotor blockage ratio, $(S/A)_{TR}$
c.g.	center of gravity
C_p	rotor power coefficient $P/\rho AV_T^3$
C_{SF}	fin side force coefficient $SF/\rho(AV_T^2)_{TR}$
C_T	rotor thrust coefficient $T/\rho AV_T^2$
C_p/C_T	tail rotor power to thrust ratio
C_{yM}	yawing moment coefficient $YM/\rho(AV_T^2R)_{TR}$
d	main rotor diameter, ft
h/d	height-to-diameter ratio
P	rotor power
s	area of the tail that is blocked by the fin, ft^2
SF	fin side force, lbs
T	rotor thrust, lbs
YM	yawing moment referenced to model c.g., ft-lbs
V	airspeed, kts
VI	main rotor average induced hover velocity, $\sqrt{T/2\rho A}$, kts
V/VI	nondimensional airspeed, $\mu/\sqrt{C_T/2}$
V_T	rotor tip speed, fps

Greek

α	vertical flow angle, positive for flow from below, deg
β	lateral flow angle, positive for flow from the right, deg
ψ	wind azimuth, positive nose right, deg.
ρ	air density, slugs/ft^3

Subscripts

TR	Tail Rotor
MR	Main Rotor
F	Fin

INTRODUCTION

Very little is known about the flow characteristics at the empennage at low speed near the ground or away from it. Even the simplest representations without the ground vortex or rotor tip vortex are not available from past research. The tail rotor as a subsystem of the helicopter is second only to the main rotor in importance. Improvements in its performance, weight and simplicity have long been among the goals of helicopter engineering. To a considerable extent, it has shared in the benefits from main rotor oriented research, but to a degree it has suffered from the emphasis on the isolated rotor context of that research. In recent years there has been a general recognition of the tail rotor's unique location and environment.

The tail rotor cannot be treated merely as a small main rotor in the overall design task. In the aera of aerodynamic design and performance there are many aspects where the tail rotor problem is different and more complex than the main rotor. The more significant differences are as follows:

- Maximum thrust requirements occur near zero airspeed where main rotor aerodynamic torque is highest. Thrust is generally shared with the fin at higher airspeeds.
- The vertical orientation of the rotational plane results in severe constraints to the diameter.
- The tail rotor and other empennage elements are placed directly in the path of the main rotor wake for most flight conditions.
- The adjacent components, i.e., fin, stabilizer and tailboom are close and of similar size and experience significant interaction with both the tail rotor and the main rotor flow fields.
- The tail rotor and empennage are placed directly in the path of the ground vortex in rearward and sideward flight.
- The variation of inflow angle encompasses a full 360 degrees thus requiring operation within the vortex ring state.

The aerodynamic coupling of the fin and the tail rotor is perhaps the most intriguing element of the empennage interactions. The problem involves the interaction of a passive and an active element. The fin/tail rotor couple has the added complications

of interacting with the complex main rotor wake through a full 360 degrees of inflow angle. Of all the potential interactional effects, the fin load has the most profound effect on tail rotor sizing and the mechanics of its generation are not fully understood. Investigations of this effect have been reported in references 1, 2, 3 and 4. The fin load appears to be a function of the aerodynamic conditions at the empennage due to the integrated effects of the relative wind speed, the wind direction, the tail rotor thrust and the main rotor thrust.

Indeed, this experimental investigation was undertaken with the objective of providing data on the tail rotor and fin loads that result from their interactions with each other with the main rotor wake at work. This investigation was conducted deep in ground effect where the ground severely deflects the main rotor wake altering the flow environment of the helicopter. The model capabilities and the technical approach employed during this investigation have provided a systematic study of the complex fluid mechanics that affect tail rotor/fin interactions.

DESCRIPTION OF THE EXPERIMENTAL PROGRAM

OVERVIEW

The experimental investigation was conducted at the Boeing Vertol V/STOL tunnel. The 20-ft by 20-ft test section was configured with the walls and ceiling removed to eliminate the need for boundary corrections at low airspeeds. The model employed for this investigation was the 1:4.85 scale YUH-61A and is shown in the tunnel in Figure 1. The main rotor is 10 feet in diameter and fully articulated. The tail rotor is 2 feet in diameter and entails a flex strap design. More detailed model parameters are given in Table 1.

Model forces and moments were measured at various wind azimuths with the main rotor and tail rotor thrusts set at predetermined values. The nominal rotor thrust coefficients for this test program were 0.0062 for the main rotor and 0.012 for the tail rotor. Variations in both main and tail rotor thrusts from these nominal values were studied at various flight conditions to determine the functional relationship between the measured aircraft loads and the operational parameters such as airspeed, sideslip and gross weight.

The test was conducted deep in ground effect at a height-to-diameter ratio of 0.35. Airspeed was varied from hover through 45 knots or transition. In this flight regime the ground plane sharply deflects the main rotor wake resulting in the formation of the ground vortex at low speeds. Near transition, however, the main rotor wake is blown aft of the model and the main rotor tip vortices are shed from left and right tips of the rotor disk. Both of these flow anomalies have a significant impact on the tail rotor and fin loads when they impinge on the empennage. The resultant variations in empennage loads and the flight conditions where they occurred are presented in this report.

As part of the closely related ATL contract, variations in tail rotor/empennage configuration were also studied. Additional insight into the influence of blockage ratio on empennage loads and tail rotor performance was provided by the investigation of varying the fin size directly. The nominal fin configuration had a blockage ratio of 0.35. An extensive data base was acquired for this fin configuration which is representative of the high blockage ratios of contemporary aircraft. Two other fin configurations were also studied. The results for all three fin configurations will be discussed in more detail later.

For the subject contract a smaller vertical fin with a rectangular planform was developed for the study of the integrated flow angles at the empennage. A variable incidence mechanism was installed to rotate the vertical fin and its associated balance.

This mechanism provided the capability to rotate the fin from + 90 degrees (leading edge to the right) to -90 degrees (leading edge to the left). Variation in fin side force as a function of fin-incidence at selected flight conditions provided a quick determination of the mean side flow angle at the empennage.

To provide additional insight into the detailed flow structure of the interactive flows, hot film and flow visualization techniques were employed. Correlation of model loads data with these detailed data verified the proximity of various flow components, i.e., main rotor wake, tail rotor wake and ground vortex, near the aircraft for conditions of high interactivity.

MODEL AND TEST STAND

The model was mounted on the Single Rotor Helicopter (SRH) test stand that provides power and all of the necessary services to the model such as hydraulics for control and oil for cooling. Figure 2 gives a detailed schematic view of the SRH stand complete with power pod, support strut, YUH-61A model and the new external tail rotor drive mechanism. Three air motors which are located in the power pod provide 400 horsepower to drive the main rotor via a shaft through the support strut. For the study of various empennage/tail rotor configurations during this test, the tail rotor was mounted on an external support structure as seen in Figure 2.

Power to the tail rotor was provided by the 52 horsepower electric motor that is mounted on the support structure (see Figure 2). Use of sophisticated electric motors provides compactness while affording precise speed control. Tail rotor collective pitch was actuated remotely to provide direct control over thrust. Being a flex strap design, variations in collective pitch were effected by elastic twist of the flex beam structure. The definition of tail rotor collective pitch therefore is the blade pitch change per unit deflection of the pitch actuator for the static, nonrotating condition. This obviously does not account for elastic wind up due to high rotational speeds during tail rotor operations. However, for this test program tail rotor thrust level is of primary concern not collective pitch.

With the addition of the external tail rotor drive mechanism to the SRH stand the fixed ground plane which is used for ground effect studies had to be modified to accommodate changes in model yaw angle. A turntable insert for the fixed ground plane was fabricated and installed as shown in Figure 2. This arrangement provided the capability to yaw the model a full 360 degrees in ground effect. The yaw drive mechanism is located in the power pod and rotates the model and external tail rotor structure about the main rotor support strut.

EMPENNAGE/TAIL ROTOR CONFIGURATIONS

Several advantages are derived from having the tail rotor mounted on a separate support structure. First, the complexity of the tail rotor drive and control mechanisms are removed from the empennage. This permits the proper simulation of component sizes as the tail boom and vertical fin need not be oversized to accommodate air hoses, hydraulic lines and data cables. Second, with the tail rotor removed from the fin, the empennage was modified to incorporate both a new fin balance and a variable fin incidence drive mechanism. Finally, the versatile design of the new balance/drive mechanism provided for the study of various fin configurations.

The baseline fin for this experimental investigation had a blockage ratio of 0.35 and provided the basis for many of the parametric studies that are presented herein. In addition, two other empennage configurations were modeled for the ATL program. The first configuration involved a smaller fin with a blockage ratio of 0.25. Figure 3 shows a comparison of the two fins. The area of the fin was reduced while holding the 1/4 chord line constant. The third configuration simply called for the removal of the fin and resulted in no blockage of the tail rotor. Some of the results that are pertinent to tail rotor/fin interactions have been included in this report for completeness.

The two fins described in the previous paragraph were not employed for the fin incidence studies because of the physical interference with the tail rotor at large fin incidence angles. Instead, a fin of short chord and equal span with zero sweep was used, see Figure 4. Its quarter-chord passed through the mean aerodynamic chord of the 35% fin. This fin had no taper and the same nose shape was used for the trailing and leading edges. With this airfoil design, the fin could rotate a full 360° to accommodate high angles of sideflow at the empennage.

INSTRUMENTATION AND FLOW VISUALIZATION

The SRH test stand is equipped with six strain gage balances to measure various model forces and moments. These balances include the main rotor, tail rotor, fuselage, empennage, fin, and total loads (which includes all loads except the tail rotor parameters). Main rotor and tail rotor power are measured separately and various other data channels are available including rotor control system settings, model orientation angles and numerous safety-of-flight quantities.

The fin balance only measures 2 quantities - side force and rolling moment. The empennage balance measures 5 components, the drag component excluded. It is important to emphasize that the

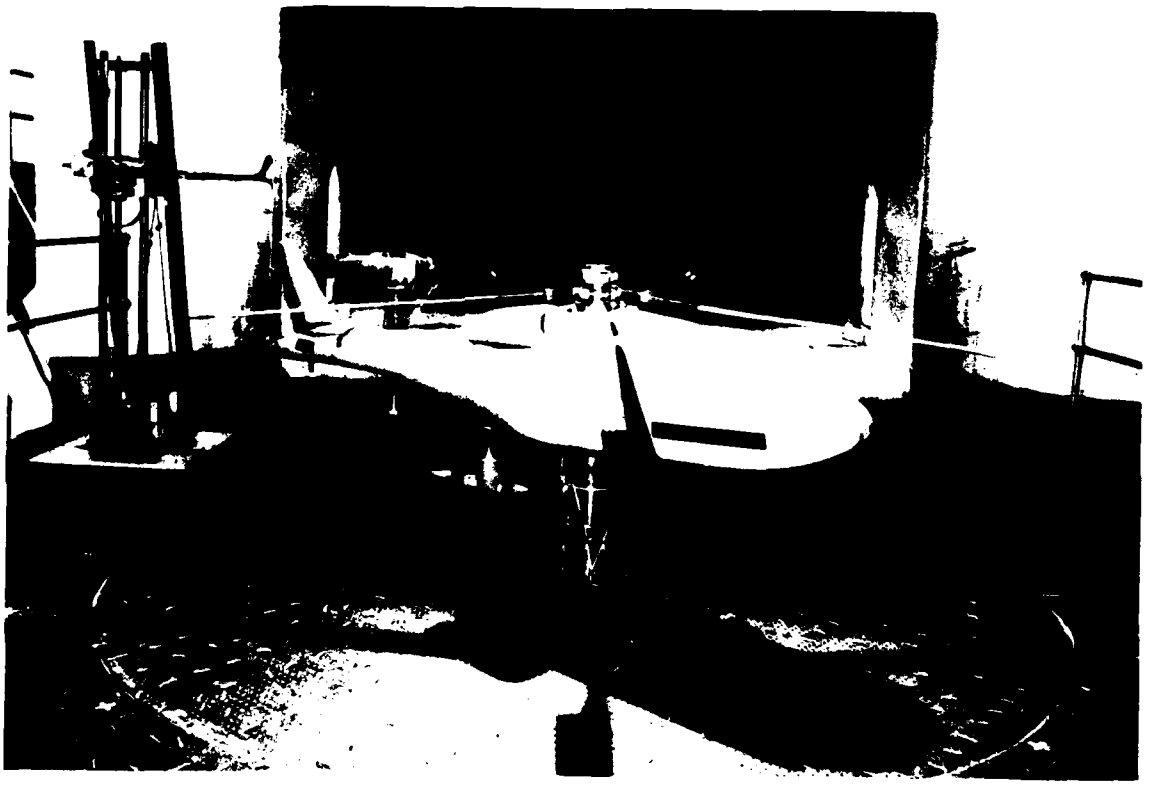

Figure 1. YUH-61A Model with External Tail Rotor Mechanism

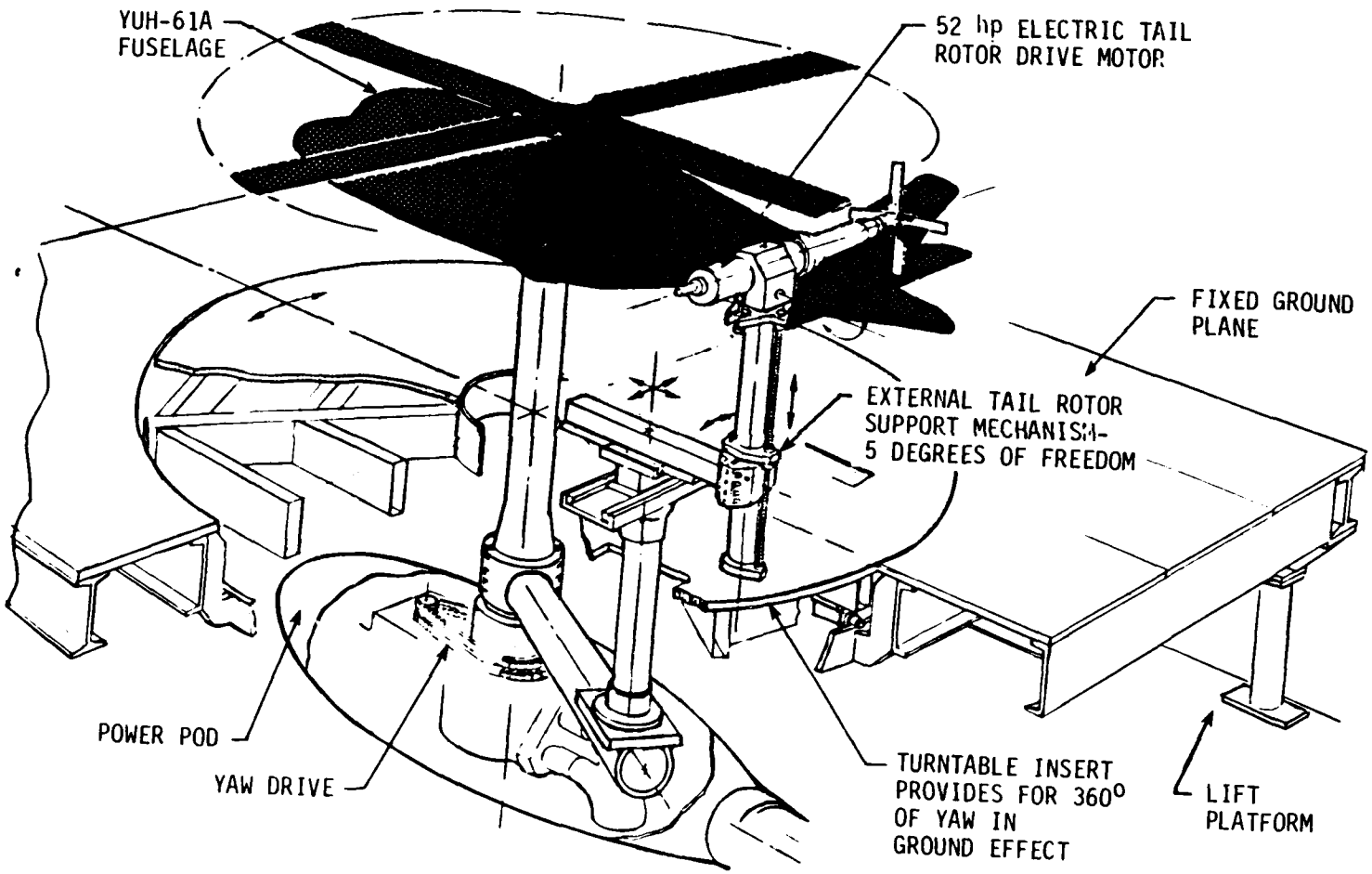

Figure 2. Sketch of Model and Test Stand Arrangement

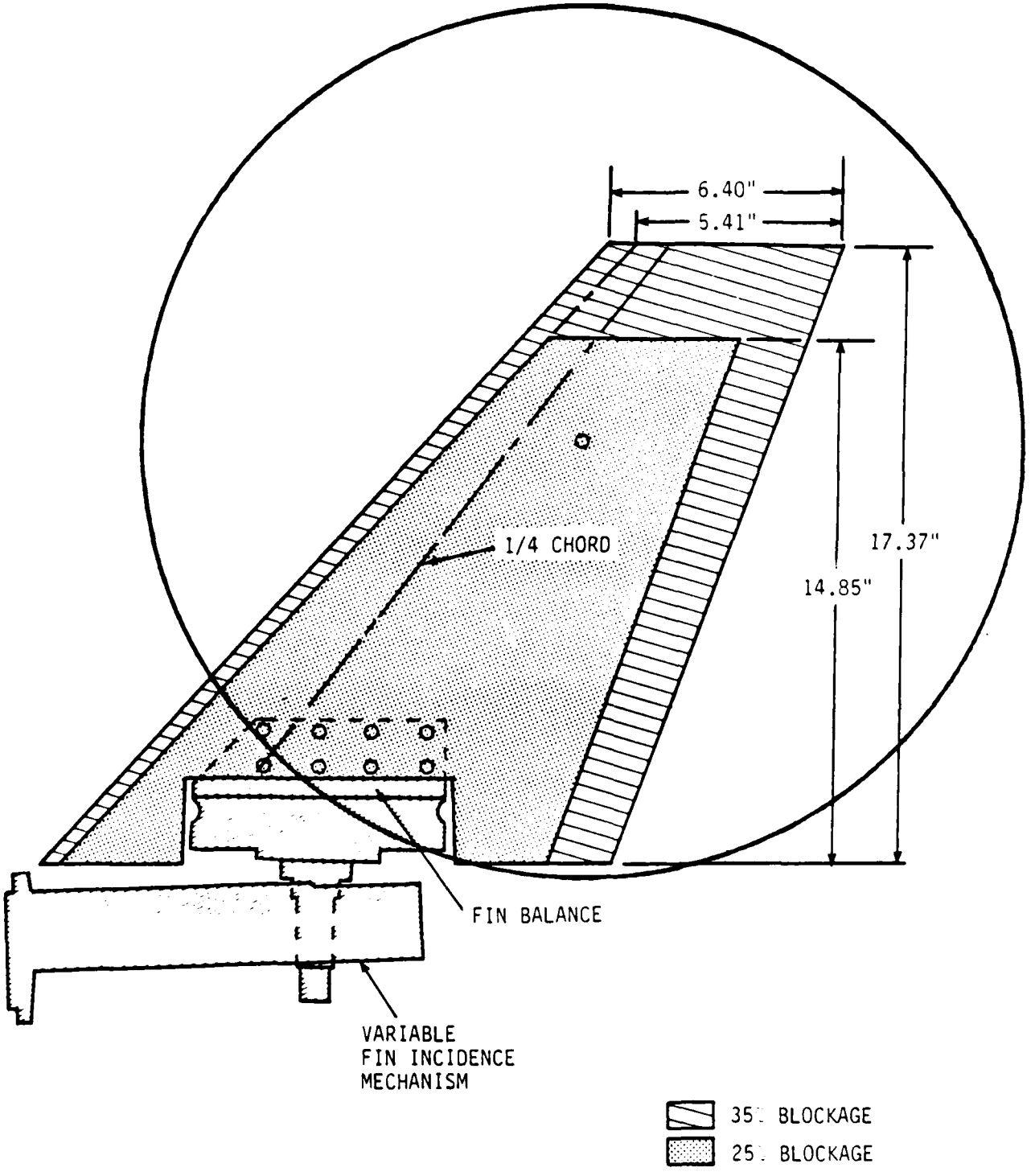

Figure 3. Interchangeable Vertical Fin

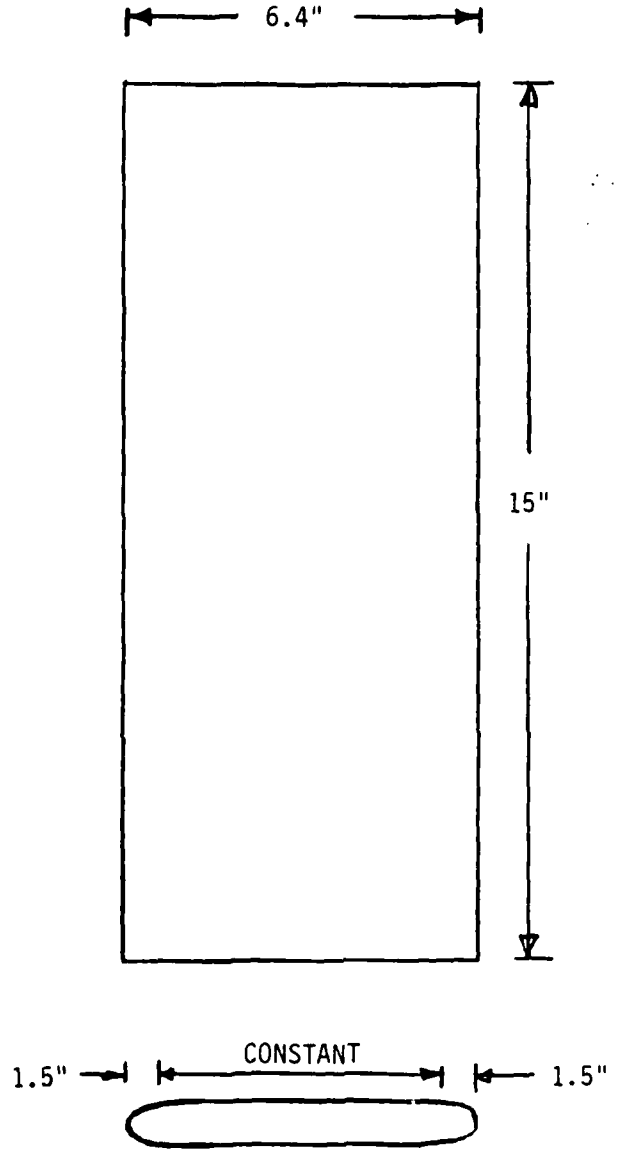

Figure 4. Rectangular, Symmetric Vertical Fin used for Fin Incidence Sweeps ($\bar{A}$ = 0.18)

TABLE 1. MODEL PARAMETERS

Main/Tail Rotors	
Airfoil Cross-Section	$VR7_{.75R}$ $VR8_{.91R}$ $VR9_{TIP}/VR7$
Rotor Radius - Main/Tail	60.62/12.50 inches
Reference Chord - Main/Tail	4.74/1.812 inches
Blade Number - Main/Tail	4/4
RPM - Main/Tail	1390/6000
Tip Speed - Main/Tail	735/648 fps
Main Rotor Shaft Incidence to WL	4 degrees forward
Main Rotor Center Station/Waterline	41.6/43.6 inches
Tail Rotor Center Station/Waterline	116.1/48.6 inches
Solidity - Main/Tail	0.0883/0.0943
Twist - Main/Tail	12.0°/0.0 degrees
Hinge Offset - Main/Tail	4.5%/0.0 (effective)
Horizontal Stabilizer	
Airfoil Cross-Section	NACA 0012
Span	40.20 inches
Mean Aerodynamic Chord (MAC)	6.87 inches
Root Chord (Extended)	8.25 inches
Tip Chord	5.15 inches
1/4 - Chord Sweep	6.8 degrees
Tail Arm (25% MAC to STA 44.3)	63 inches
Incidence	45 degrees
Vertical Tail	
Airfoil Cross-Section	NACA 63_4 - 421
Blockage Ratio	35% / 25%
Height (Tip to WL 37.5) - 35/25%	17.37/14.85 inches
Root Chord - 35/25%	15.2/13.46 inches
Tip Chord - 35/25%	6.4/5.41 inches
Mean Aerodynamic Chord (MAC)	11.4/10.4 inches
1/4 - Chord Sweep - 35/25%	37.5/37.5 degrees
Tail Arm (25% MAC to STA 44.3) - 35/25%	66.9/65.9 inches
Incidence - 35/25%	0/0 degrees

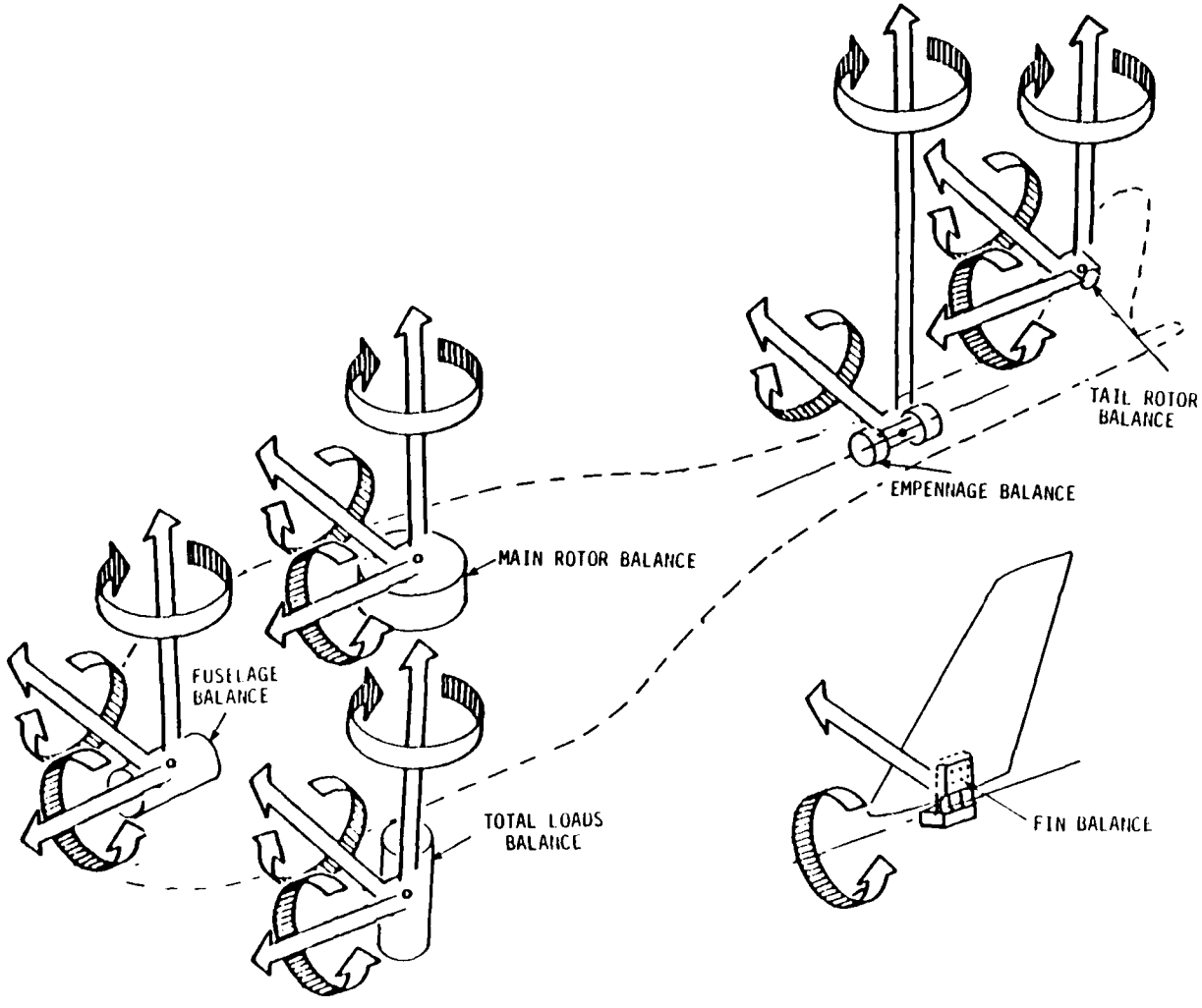

Figure 5. Balance Orientations

DISCUSSION OF RESULTS

VARIABLE INCIDENCE FIN

The vertical fin incidence was remotely actuated to facilitate the determination of the mean sideflow angle at the empennage. With the trend toward large fins on contemporary helicopters, the variable incidence fin may be the solution to the adverse fin force problem just as the programmed variable incidence horizontal stabilizer has been universally adopted as the solution to the transition download problem. The effect of varying fin incidence on fin side force is shown in Figures 6 and 7.

The mean sideflow at the empennage is the sum of the free stream flow, the main rotor downwash, the tail rotor side flow and the fuselage flow field. Figure 6 shows the fin incidence that is required for a zero fin sideforce condition at varying levels of tail rotor thrust. At low tail rotor thrusts large negative (leading edge turned to the left) angles are required. Since the model is pointed into the wind this negative incidence angle results from the sidewash induced at the fin due to swirl component of the main rotor wake. As the tail rotor thrust increases the tail rotor sidewash offsets the swirl induced by the main rotor resulting in lower incidence angles for zero fin force.

Figure 7 is a plot of the fin incidence required for zero fin force as a function of main rotor thrust. Increases in main rotor thrust result in higher negative incidence angles due to the increased sidewash. It must be noted that these tests were conducted deep in ground effect (h/D=0.35) where changes in main rotor thrust at a given airspeed have a significant effect on the total flow environment of the model. Although the wake blow-back angle will change with main rotor thrust a sideward flow component will still be induced at the empennage. The variations in wake structure as a function of airspeed and disk loading will be discussed in more detail, later in the report.

Adverse Fin Sideforce

Figures 8 and 9 show the effects of tail rotor and main rotor thrust, respectively, on fin force for a 35 knot wind from the right. For these runs the fin incidence was fixed at zero degrees. As a result the fin force indicates the change in the integrated sideward flow at the empennage. In both figures the fin force becomes more adverse as either rotor thrust is increased. From the sign conventions established in Figure 5, a negative fin force is opposite the thrust of the tail rotor and thus adverse. In Figure 8 the buildup of adverse fin loads is primarily associated with the negative pressurization of the near side of the vertical fin by the tail rotor inflow. This depres-

surization of the fin surface is a primary source of adverse fin loads and is discussed in greater detail in reference 1.

Figure 10 shows the effects of airspeed on fin side force for different levels of tail rotor thrust in right sideward flight. In this case, the fin incidence was fixed at 90 degrees thus aligned with its chord parallel to the free stream flow. The curves for all three plots exhibit a very flat variation with tail rotor thrust. This insensitivity to tail rotor thrust is due to the reduced blockage ratio, that is the area of the tail rotor disk that is blocked by the vertical fin, with the fin rotated 90 degrees. Figure 10 shows that the adverse fin force builds up abruptly as airspeed is increased, particularly in ground effect. Below transition the roll up of the main rotor wake dominates the flow environment of the empennage. For the 0 and the 20 knot wind cases the empennage is immersed in the wake. However, above 30 knots the main rotor wake is blown aft and the free stream flow impinges on the empennage directly thus accounting for the sudden increase in the overall fin side force level between 20 and 30 knots.

Finally, the profound effect that fin incidence can have on adverse fin load is shown in Figure 11. Again, for a 35 knot right sideward flight condition the measured fin side force is compared for two fin incidence conditions; zero and 90 degrees. Several important results arise from this comparison. First, the fin side force is not zero for the case where the fin incidence is 90 degrees because of the total integrated effects of free stream, main rotor, tail rotor and fuselage flow fields. Second, a substantial increase in fin sideforce is measured at all levels of tail rotor thrust caused by changing the fin incidence. As noted earlier, this change in fin incidence results in a change in blockage ratio. As the area of the fin that is exposed to the inflow of the tail rotor is increased so does the negative pressurization of the fin surface also increase. In a similar manner, the area of the fin that is exposed to free stream flow is also increased for a fin incidence of zero. The third observation is that the gradient or rate at which the side force builds up with increasing tail rotor thrust is much greater for the higher blockage ratio condition or zero fin incidence.

The fin, in turn, also affects the tail rotor. Figure 12 is a plot of the tail rotor power required to maintain a constant thrust level for the two cases of fin incidence shown in the previous figure. Both curves show the characteristic increase in power with tail rotor thrust. The most striking feature is the lower power required for zero fin incidence condition or higher blockage ratio. This effect has been called the "ceiling effect." Apparently, the higher blockage ratio fin configuration results in lower average inflow velocities through the tail rotor

disk due to free stream flow. In a sense the tail rotor is in less of a climb condition thus resulting in lower power.

INTERACTIONS WITH THE MAIN ROTOR WAKE

The rectangular fin in concert with the variable incidence fin mechanism provides some insight into the complex interaction between the fin and the tail rotor. Most significantly the blockage ratio was seen to have a strong impact on the aerodynamic coupling of these two components. For that reason, the majority of the subject test program was conducted with the nominal YUH-61A fin configuration at a blockage ratio of 0.35. This is representative of the large fins being employed by contemporary aircraft. To study the effects of the main rotor wake on empennage loads a fine grain yaw sweep was conducted for a wind magnitude of 30 knots.

Figure 13 shows the fin side force as a function of wind azimuth for two levels of tail rotor thrust. It is important to note that the tail rotor thrust was held constant as opposed to holding tail rotor collective pitch fixed as was done is previous investigations (see references 2 and 3). As was shown in the previous section the fin side force is very sensitive to variations in tail rotor thrust. Therefore, testing at fixed tail rotor thrust precludes the effects of changing inflow at the tail rotor due to changes in wind azimuth.

As a result, the variations in fin side force illustrated in Figure 13 are due to the interaction between the fin and the detailed flow structure of the main rotor wake. For example, at wind azimuths near 45 and +50 degrees very large and abrupt changes in fin force occur over very narrow ranges of wind azimuth. Hot film measurements show that these variations in fin force are attributed to the interaction with the main rotor tip vortices which are blown aft and into the empennage for a 30 knot wind condition (at a main rotor thrust coefficient of 0.0062). Moreover, Figure 13 shows that a maximum adverse fin force (largest negative value) occurs at a wind azimuth of 45 degrees and not 90 degrees or right sideward flight as expected. In fact, Figure 14 shows that the maximum adverse fin force can be as large as 40 to 60 percent of the tail rotor thrust.

The results shown in Figures 13 and 14 show how stongly the aerodynamic interactions of the various flow components with the aircraft can affect its handling qualities, particularly in the directional axis. To further emphasize the significance of fin force on the aircraft loads Figure 15 shows a breakdown of the total airframe yawing moment as a function of wind azimuth into its two primary components, empennage and fuselage. In this report, the term fuselage is that portion of the airframe ahead of the empennage balance, see Figure 5. Due to the large fin and

the distance from the reference center of gravity, the empennage, or more importantly the fin, clear dominates the makeup of the total airframe yawing moment. This characteristic, however, is very dependent upon the specific fuselage shape.

In a similar fashion as the fin, the tail rotor is also influenced by the main rotor wake. Similar nonlinear variations in tail rotor power to thrust ratio occur near -45 and +50 degrees as shown in Figure 16. The effect of the main rotor tip vortex on tail rotor power appears to be greater at ψ = +50 degrees (left sideslip) compared to ψ = -45 degrees (right sideslip). This result indicates that the fin, to some degree, can shield the tail rotor from flow anomalies such as a main rotor tip vortex much like the way it changes the average inflow velocity in right sideward flight (see Figure 12).

In addition to model loads data, flow visualization was employed to gain a detailed view of the flow over the fin. Tuft formations on the side of the fin which is closest to the tail rotor are presented in Figures 17, 18 and 19. The wind azimuth is different for each figure however, the wind magnitude remained constant at 30 knots. In all cases, the tufts become somewhat more erratic (as indicated by the blurred tufts) and begin to raise off of the fin surface as the tail rotor thrust is increased. This phenomenon occurs even in left sideward flight conditions where the free stream flow opposes the tail rotor flow thus illustrating the influence that the tail rotor exerts on the fin in close proximity.

Hot film flow measurements were employed to identify and locate the main rotor tip vortex near the empennage. The hot film probe was located just upstream of the empennage as shown schematically in Figure 20. The probe was aligned with the free stream flow; therefore, the measured flow angles are relative to the probe axes. Figures 21, 22 and 23 show some of those results for vertical sweeps of the hot film probe just ahead of the empennage and tail rotor for a wind azimuth of -50 degrees (right sideslip). For the 30 knot wind condition the probe virtually passes through the center of the main rotor tip vortex. At a model waterline of 50 inches the vertical flow angle approaches zero as the lateral flow angle dramatically changes sign. This abrupt change in lateral flow angle is characteristic of vortical flow. Moreover, Figure 23 shows that the main rotor tip vortex is very strong and its flow structure changes very little for large changes in tail rotor thrust.

PARAMETRIC VARIATIONS AT SELECTED WIND AZIMUTHS

In recent years, helicopter flight close to the ground has gained increasing importance particularly in Nap-of-the-Earth (NOE) terrain following maneuvers. Helicopter flight near the ground,

however, is very complex due to the presence of the ground vortex. The formation and structure of the ground vortex has been the subject of several investigations particularly with respect to its effects on helicopter directional control. Specific programs are documented in references 2, 3, 4 and 5. In fact, any study of helicopter aerodynamics in ground effect at low airspeeds must address the effects of the ground vortex on aircraft loads. References 6 and 7 discuss some of the operational considerations pertaining to the passage of the ground vortex.

During this investigation the ground vortex was found to influence the tail rotor/fin interactions throughout the transition speed regime for wind azimuths ranging from +90 (left sideward flight) through 180 to -90 degrees (right sideward flight). The precise characterization of the ground vortex as a function of airspeed and main rotor thrust is documented in reference 1 for this investigation. Figure 24 shows the ground vortex as it approaches the empennage for a 20 knot wind from the right. Presented in Figures 25 through 31 are the resultant model loads that were measured at the four principal wind azimuths of 0, +90, 180 and -90 degrees for the speed range from 0 to 45 knots. The data presented in the previous sections showed the significance of both main rotor and tail rotor thrust condition on fin side force. Therefore, to provide further insight into the functional relationship of the tail rotor/fin aerodynamic interactions speed sweeps were conducted at various levels of main rotor and tail rotor thrust.

The variation in fin side force as a function of airspeed at the four principal wind azimuths is given in Figure 25. It was shown in reference 1 that the ground vortex formed under the leading edge of the main rotor at a nondimensional airspeed of 0.6 or 15 knots. Subsequently, the ground vortex disappeared at a nondimensional airspeed of 1.25 or 30 knots by rolling up into the main rotor tip vortices. For nondimensional airspeeds [illegible] 1.[illegible] the ground vortex passes over the empennage and [illegible] rotor resulting in large variations in component loads as shown in Figure 25. For example, in right sideward flight, Figure 25b, the passage of the ground vortex near the empennage resulted in a large buildup of adverse fin sideforce at a nondimensional airspeed of 1.05.

In addition to varying airspeed, three levels of tail rotor thrust were studied. Close examination of Figure 25 shows that the effects of the ground vortex on fin side force are not affected noticeably by the change in tail rotor loading. However, in all four wind azimuth conditions the fin side force is more adverse, that is more negative, at every airspeed for increasing tail rotor thrust. Again, this is primarily due to tail rotor pressurization of the fin.

A comparison of the relative magnitudes of the fin force at the four wind azimuths is presented in Figure 26. In this case the tail rotor thrust coefficient is a constant 0.012; the nominal condition for this test. Figure 26 clearly shows the abruptness of change in fin side force that is experienced in both left and right sideward flight compared to the other two flight conditions. In addition, it is obvious that the most severe adverse fin force occurs in right sideward flight (ψ = -90°) as airspeed approaches transition. In contrast, favorable fin loads are measured for the same speeds in left sideward flight. The remaining two flight conditions exhibit much smoother variations in fin force over the transition speed regime.

It is interesting to note that the four curves shown in Figure 26 come together at low advance ratios. This is not unusual as the main rotor wake dominates the flow environment of the helicopter at very low airspeeds thus minimizing any asymmetry in the flow field at the empennage due to free stream flow effects. However, as expected, the assymmetry quickly evolves as airspeed is increased. In fact, above transition, or a nondimensional airspeed greater than 1.25, the free stream impinges directly on the empennage and tail rotor having its maximum influence.

Main Rotor Thrust Effects

The correlation between analysis and experiment which is presented in reference 5 shows that the strength of the ground vortex is approximately equivalent to the summation of all of the individual blade tip vortices between the rotor and the ground. Therefore, the strength of the ground vortex is a function of the main rotor loading. The effects of varying main rotor thrust on empennage and tail rotor loads were studied for the right sideward and the rearward flight conditions. The corresponding fin side force and tail rotor power variations are shown in Figures 27 through 30. The component loads are plotted as a function of nondimensional airspeed.

Figures 27 and 29 show the same abrupt variation in fin side force near a nondimensional airspeed 1.05 and 1.0, respectively, that was seen in Figures 25b and 25d. Two important considerations emerge from the results shown in Figures 27 and 29. First, the variations in fin force become more severe as the strength of the ground vortex increases with main rotor thrust. These variations in main rotor thrust are representative of either changes in gross weight for a given configuration or a change in configuration which results in a higher disk loading. In either case the increased variation in fin force associated with increased ground vortex strength would impact the control required for trim.

Second, the data given in Figures 27 and 29 show that the maximum effects of the ground vortex occur at the same nondimensional airspeed regardless of main rotor loading (for a fixed h/D condition). Correlation of flow visualization smoke patterns with model loads data show this nondimensional airspeed to correspond to the passage of the ground vortex near the empennage. It is important to realize here that the dimensional airspeed at which these abrupt changes occur is significantly higher for higher main rotor thrust conditions. This fact is especially important to the pilot who only knows his airspeed in knots and is concerned with the safe operation of his aircraft, particularly in such close proximity to the ground. It should be remarked here that similar variations in horizontal stabilizer vertical forces were measured due to the passage of the ground vortex. These variations would affect the longitudinal axis as much as fin force affects the directional axis.

Figures 28 and 30 show the corresponding variations in tail rotor power to thrust ratio for the right sideward and rearward flight conditions, respectively. Once again, the passage of the ground vortex results in abrupt changes in the component loading. In right sideward flight the tail rotor power (Figure 28) increases substantially, almost 20 percent for the nominal thrust condition (C_TMR = 0.0062). Figure 31 provides a comparison of the tail rotor power to thrust ratio for the four principal wind azimuths over the transition speed regime. Since these tests were conducted at constant tail rotor thrust the variations in the power to thrust ratio simply reflect the changes in tail rotor power required. It is apparent from Figure 31 that the effects of the ground vortex are greatest at plus and minus 90 degrees of wind azimuth with lesser influence at 180 and 0 degrees.

FIN CONFIGURATION

For the tail rotor power critical, right sideward flight condition the effect of varying fin size was studied. The 35 percent blockage fin provided the baseline configuration. A reduced size fin with a 25 percent blockage (see Figure 3) and a fin off configuration were studied. The buildup in blockage ratio from 0 through 35 percent is representative of the design trend toward larger vertical fins. This trend has been driven by the contemporary operational requirement for satisfactory directional trim characteristics during a tail-rotor-off condition.

The increase in adverse fin force, more negative, is shown in Figure 32. The fin force is zero for the fin off condition. With the fin on, the increase in fin force at low speeds, below 0.6 nondimensional, is primarily due to the increase in the fin area that is exposed to the inflow field of the tail rotor. At these low airspeeds, the free stream flow has little effect on empennage loads. However, at the high wind speeds the main rotor wake

is blown aft and the free stream flow impinges on the empennage directly. This accounts for the large buildup in adverse fin loads for airspeeds greater than 1.25 nondimensional due to increasing fin size. Finally, in the regime where the influence of the ground vortex is greater, the larger fin exhibits a much steeper gradient. This indicates that the larger fin is more susceptible to aerodynamic interactions with primary flow components such as the ground vortex.

Figure 33 shows that fin configuration has a profound effect on the tail rotor power coefficient. Comparison of the fin off and the 35 percent blockage fin shows that the increased inflow through the tail rotor for a reduced blockage configuration resulted in higher power required. The reduced size fin, however, experienced the highest tail rotor power required of all three configurations. This is probably a result of the redistribution of the inflow over the tail rotor disk plane attributed to the change in fin shape. Further studies must be conducted to determine the affects of fin shape on tail rotor performance more precisely and to verify the trends presented herein.

MAIN ROTOR POWER VARIATIONS

Effects of Wind Azimuth

The preceding results clearly show the effects of main rotor wake on tail rotor/fin interactions, particularly the effects of the main rotor tip and the ground vortices. However, the tail rotor flow can have a significant effect on the main rotor. Figure 34 shows the main rotor power required to maintain a nominal main rotor thrust coefficient of 0.0062 as a function of wind azimuth. The wind speed is 30 knots and two levels of tail rotor thrust are presented.

The highest main rotor power required occurred in rearward flight, as would be expected. In this flight condition the free stream flow blows the tail rotor flow back into the main rotor. As it gets rolled up into the tip vortex structure the main rotor power increases. In rearward flight an increase in tail rotor thrust results in higher main rotor power. Otherwise, with the exception of ψ = +80 degrees, the main rotor power is not sensitive to changes in tail rotor thrust.

Figure 34 also shows some nonlinear perturbations in the main rotor power at 50 and +30 degrees of wind azimuth. These are very close to the wind azimuths where the main rotor tip vortices impinge on the fin and tail rotor. For the right sideslip condition the main rotor power reaches its absolute minimum at -50 degrees as the tail rotor flow blows the nearby main rotor

tip vortex downstream. In contrast, the main rotor power grows dramatically at wind azimuths of +20 and +40 degrees. Not only are these the second highest main rotor power required conditions but it is worse than the left sideward flight condition (ψ = +90°). In this condition the tail rotor wake has its strongest influence on the main rotor tip vortex that is shed from the left rotor tip. In left sideward flight (ψ = +90°) the tail rotor and main rotor tip vortex are no longer in the same longitudinal plane.

Parametric Variations at Selected Wind Azimuths

Figure 35 shows the main rotor power as a function of nondimensional airspeed for the four principal wind azimuths of 0, 90, 180 and +90 degrees. Data were obtained for three levels of tail rotor thrust coefficient ranging from 0 to 0.015 maximum. In general the main rotor power decreased with increasing airspeed as is typical of rotor performance during transition. The effects of tail rotor thrust on tail rotor/main rotor interactions is shown in Figure 35. For example, the forward flight case (Figure 35a) shows virtually no sensitivity to tail rotor thrust whereas the rearward flight condition (Figure 35c) shows a substantial increase in main rotor power required over most of the transition speed regime. The right and left sideward flight cases shown in Figures 35b and 35d show varying degrees of sensitivity to tail rotor thrust.

A comparison of the main rotor power measured at the four selected wind azimuths is shown in Figure 36 for the nominal tail rotor thrust condition. The highest main rotor power required occurs in rearward flight over most of the transition speed regime as was indicated for the 30 knot yaw sweep data shown in Figure 34.

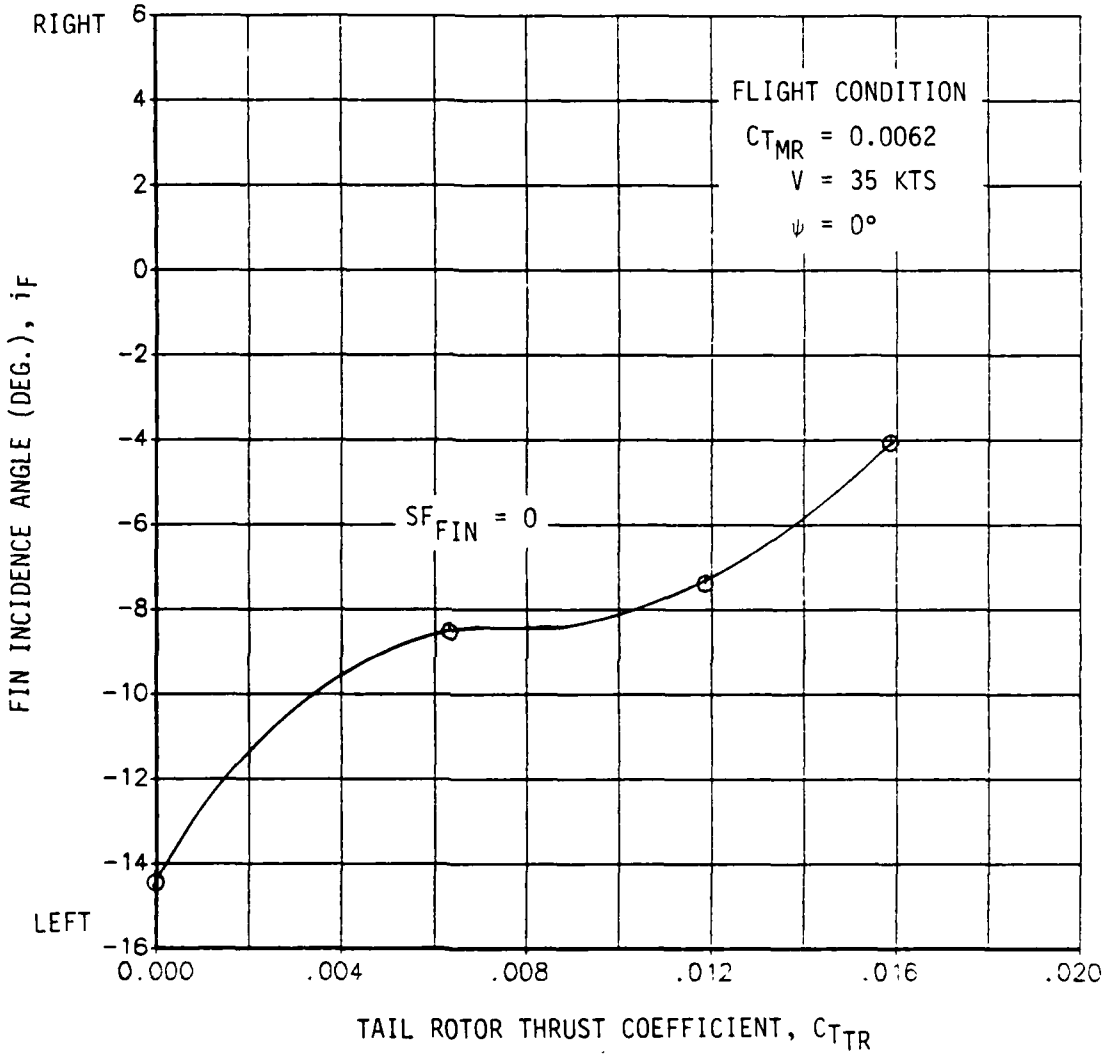

Figure 6. Variation in Fin Incidence Angle Required for Zero Fin Side Force as a Function of Tail Rotor Thrust

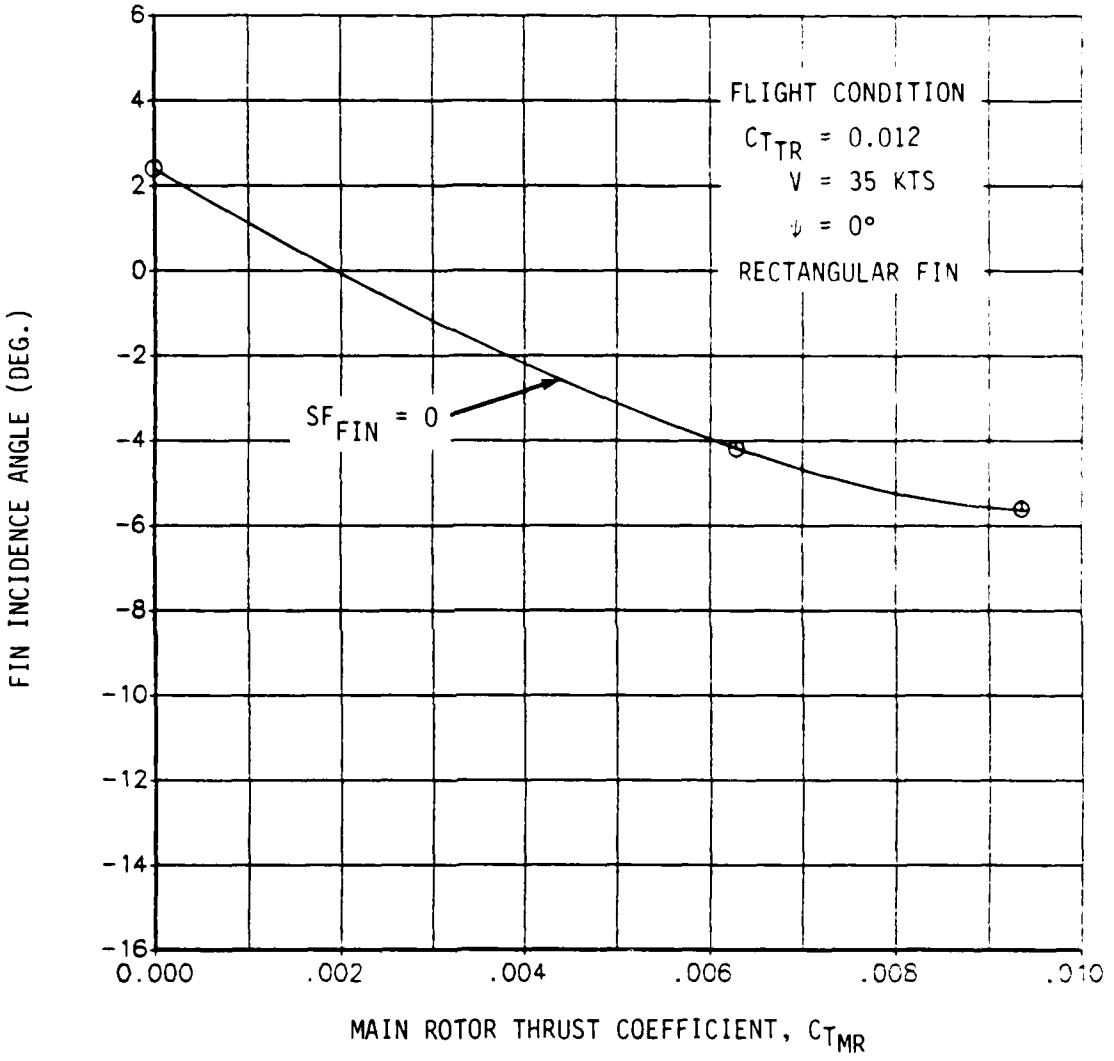

Figure 7. Variation in Fin Incidence Angle Required for Zero Fin Side Force as a Function of Main Rotor Thrust

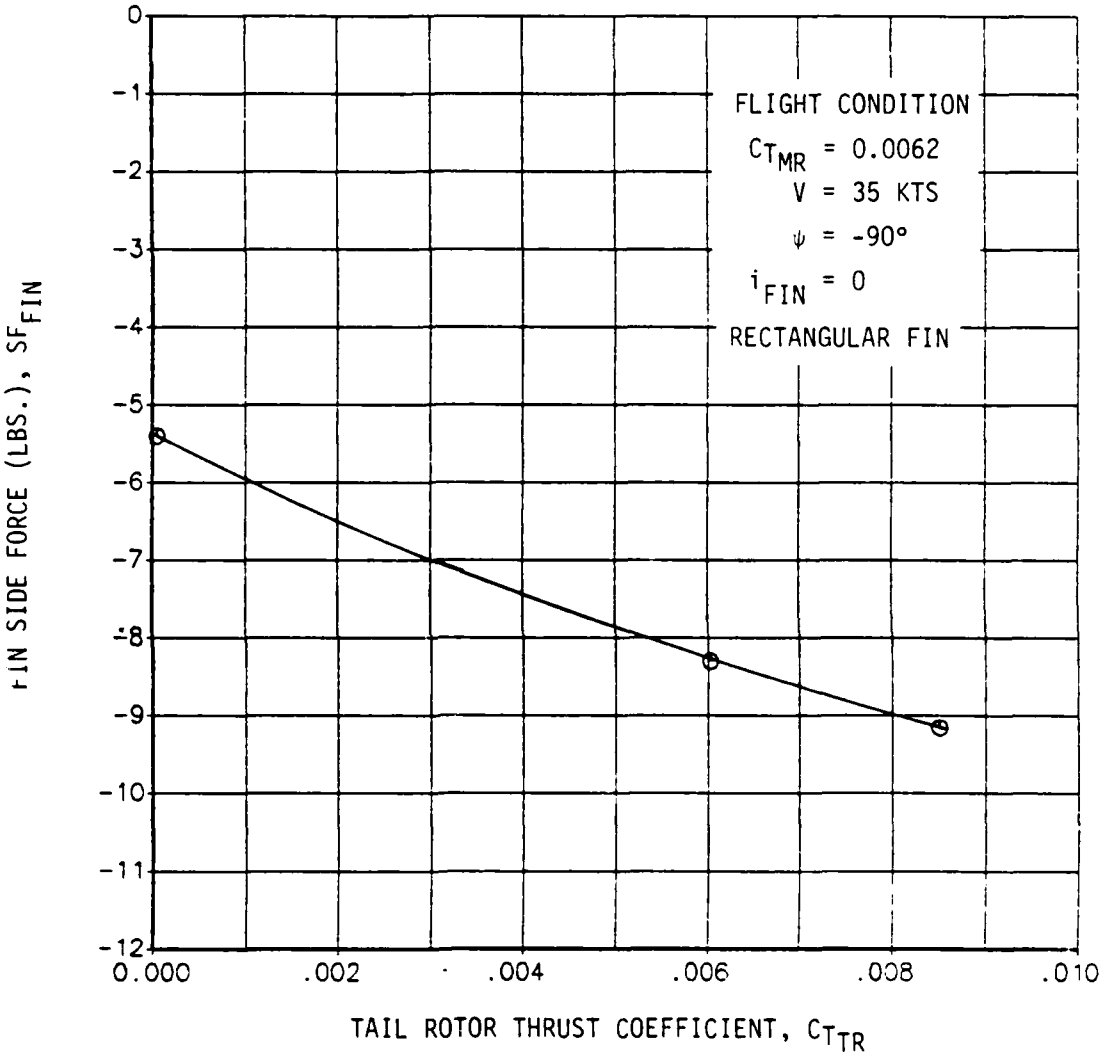

Figure 8. Effect of Tail Rotor Thrust on Fin Side Force in Right Sideward Flight (i_{FIN} = 0)

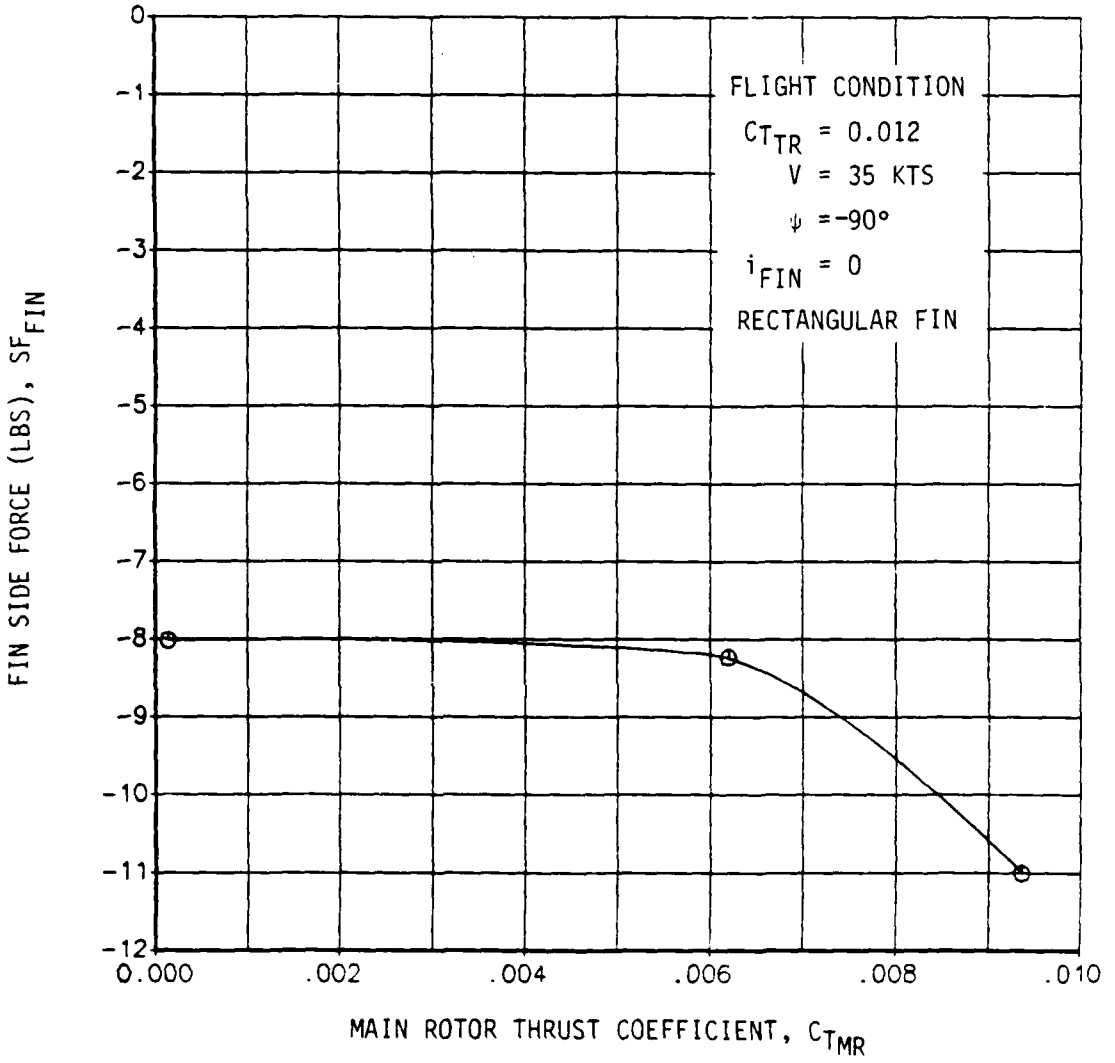

Figure 9. Effect of Main Rotor Thrust on Fin Side Force in Right Sideward Flight (i_{FIN} = 0)

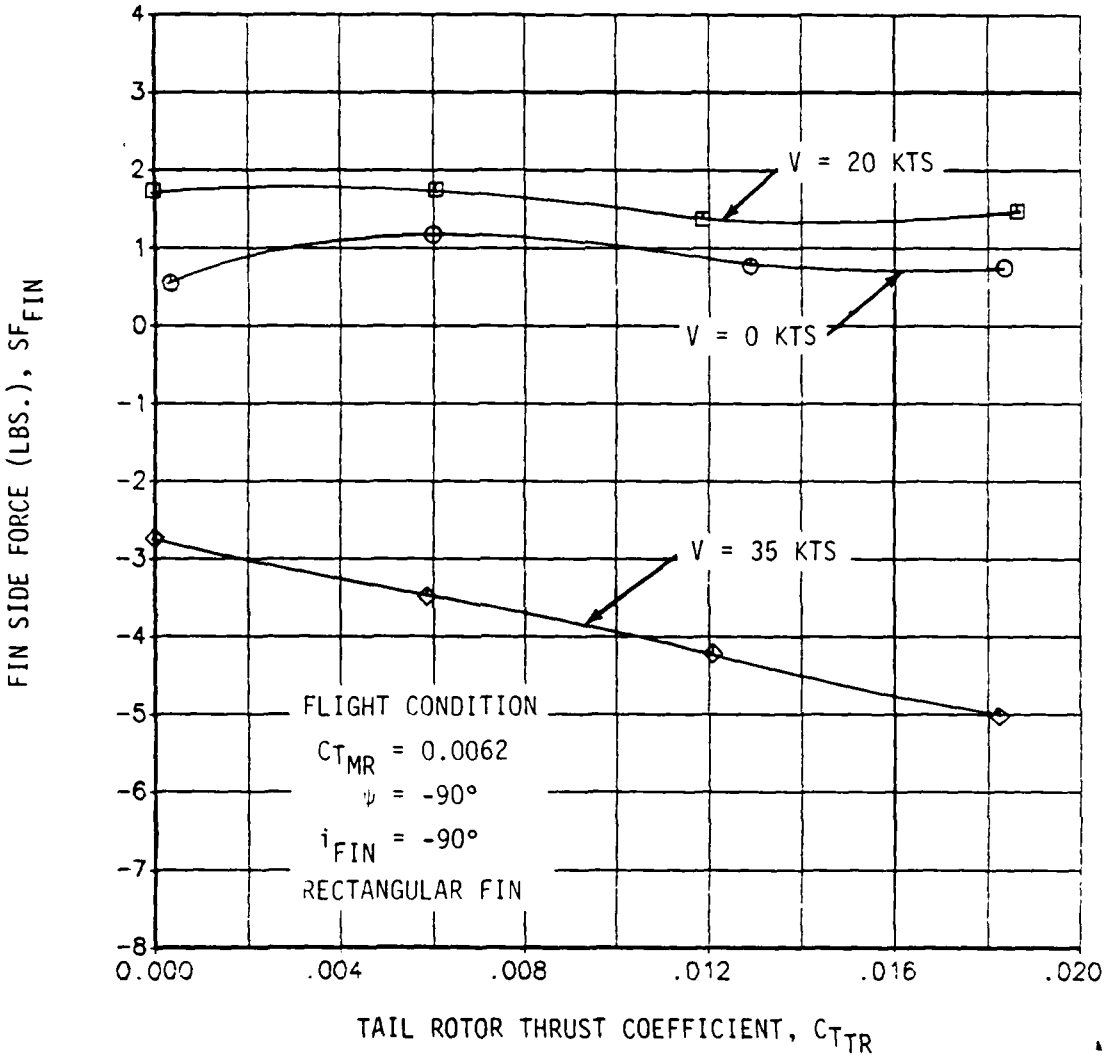

Figure 10. Effect of Tail Rotor Thrust on Fin Side Force for Different Airspeeds in Right Sideward Flight (i_{FIN} = -90°)

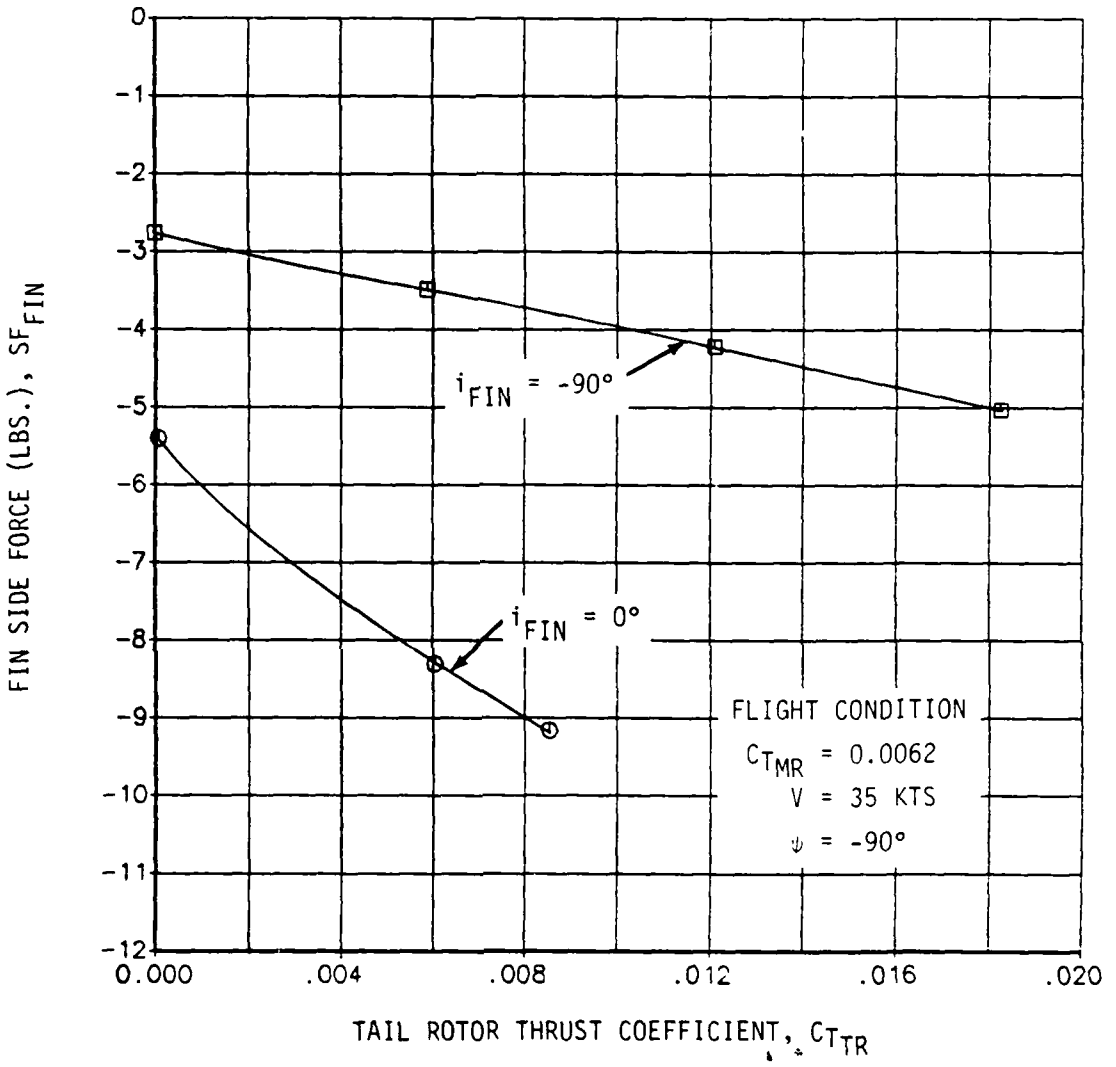

Figure 11. Effect of Varying Fin Incidence on Fin Side Force in Right Sideward Flight

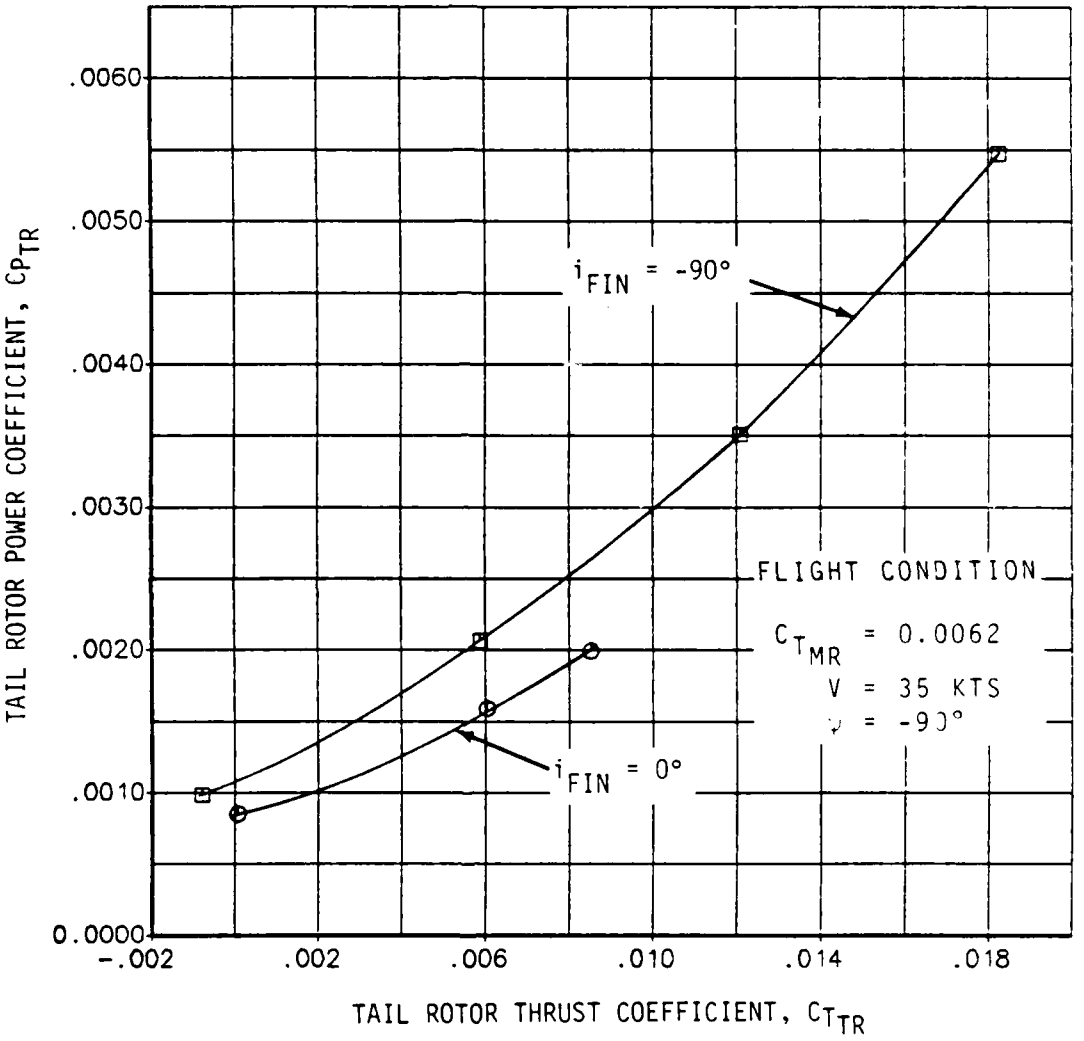

Figure 12. Effect of Varying Fin Incidence Angle on Tail Rotor Power in Right Sideward Flight

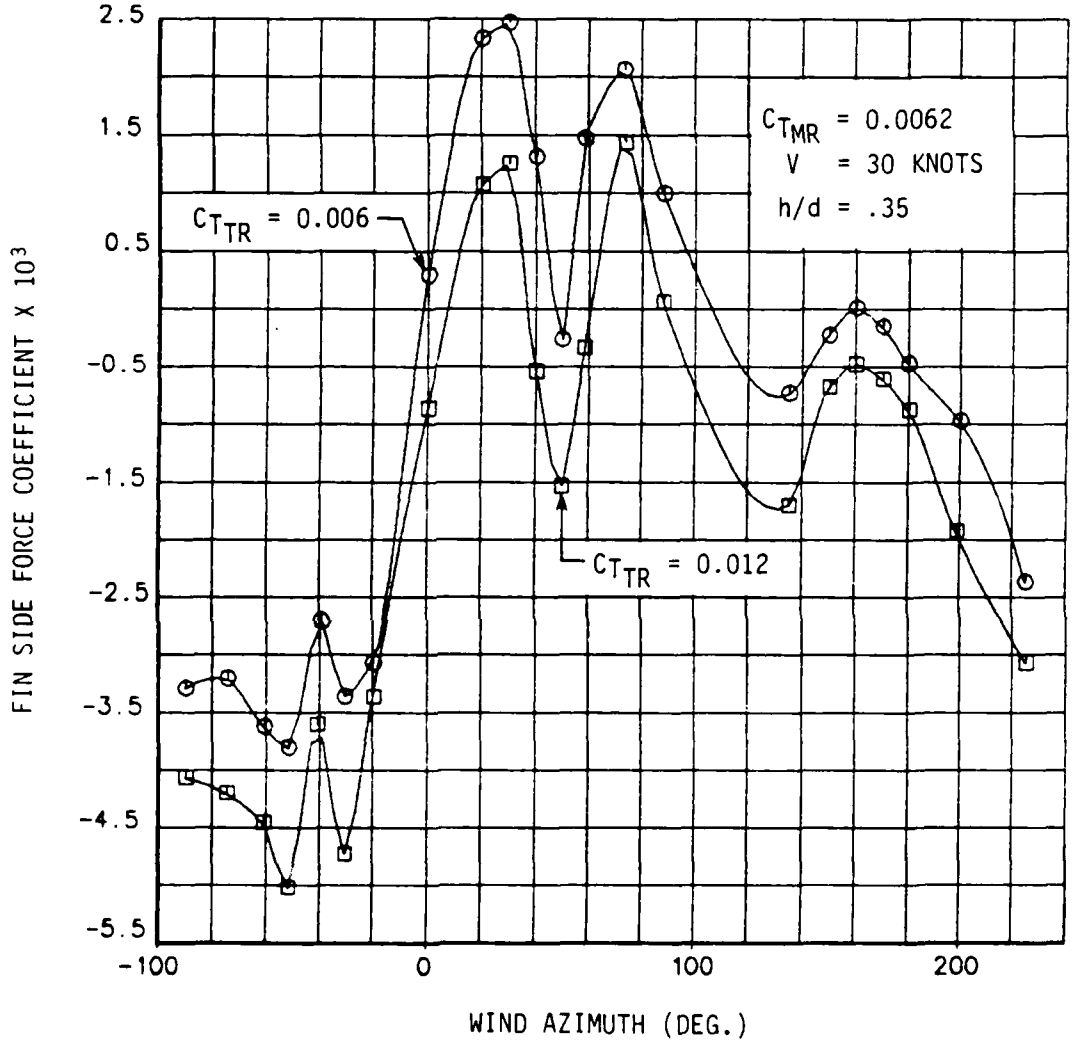

Figure 13. Effects of Wind Azimuth and Tail Rotor Thrust on Fin Side Force Coefficient.

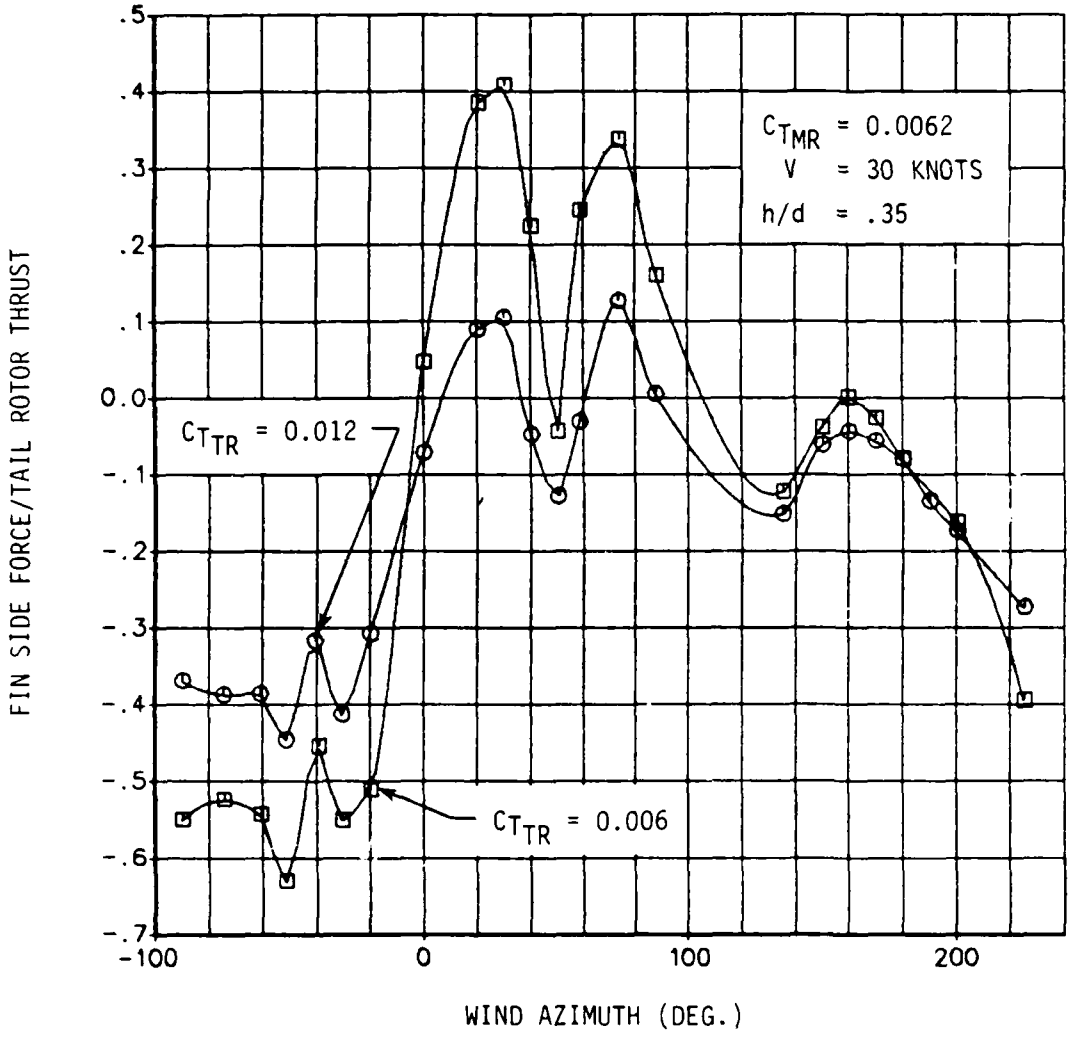

Figure 14. Variation in the Fin/Tail Rotor Force Ratio with Tail Rotor Thrust and Wind Azimuth

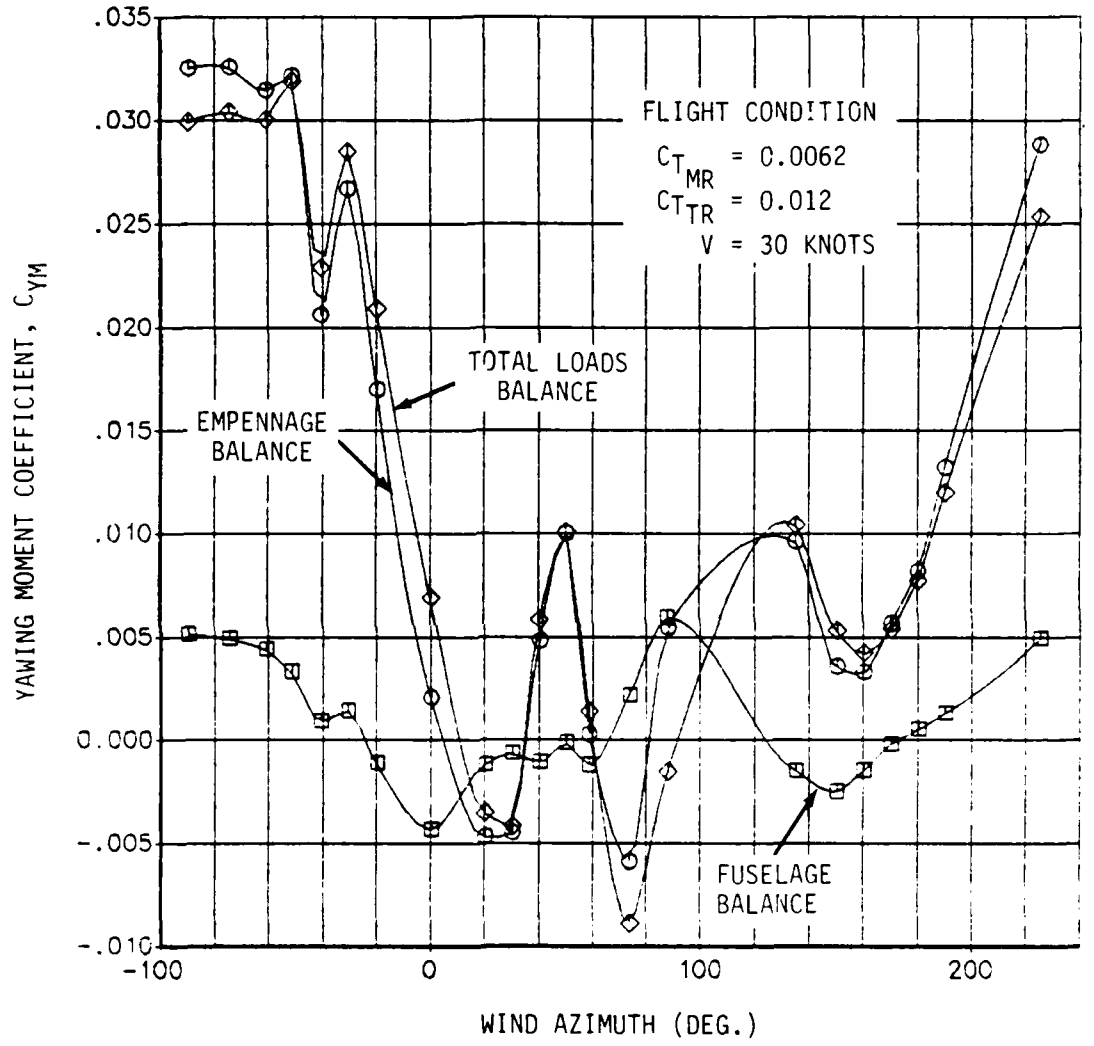

Figure 15. Component Breakdown of Yawing Moment Contributions as a Function of Wind Azimuth (referenced to model c.g.)

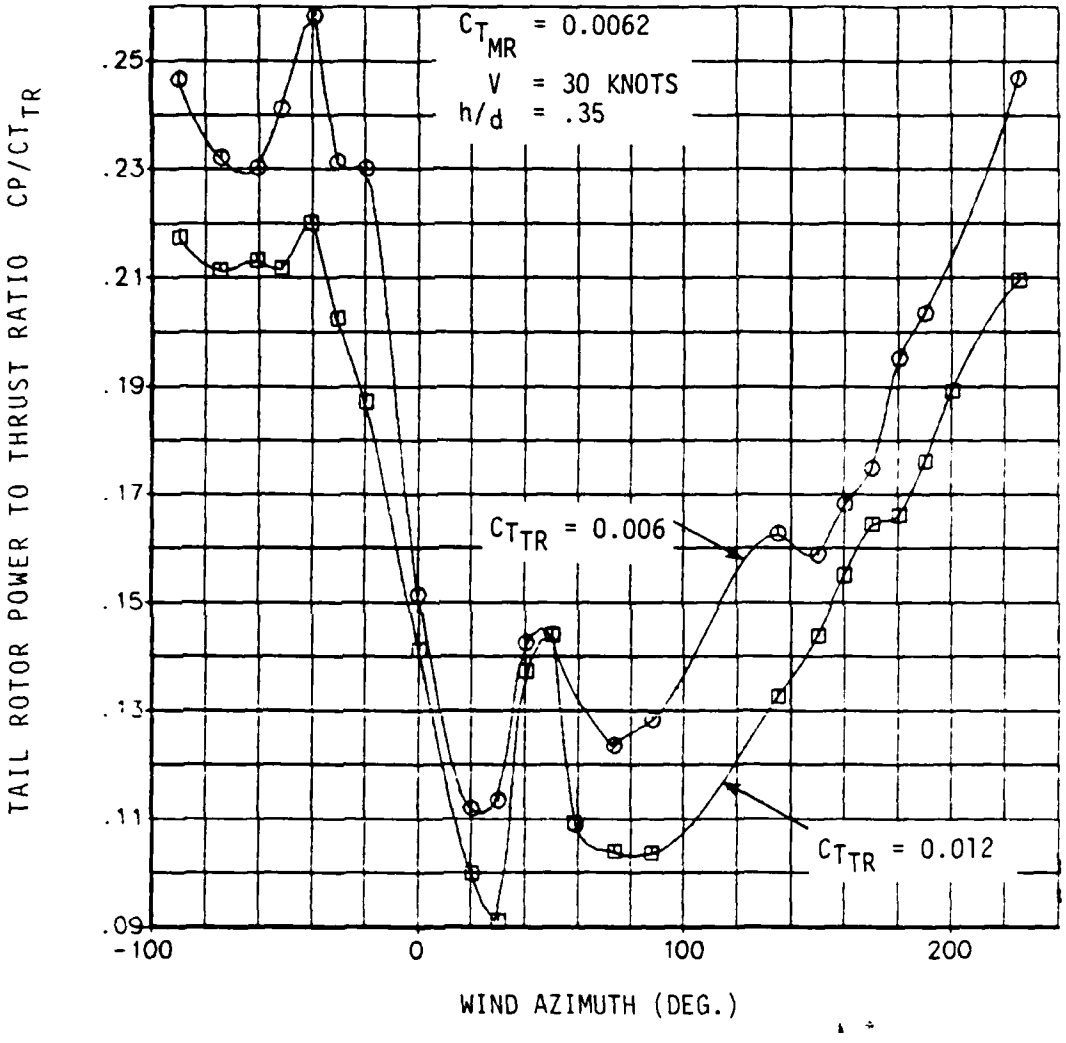

Figure 16. Variation of Tail Rotor Power Ratio as a Function of Wind Azimuth

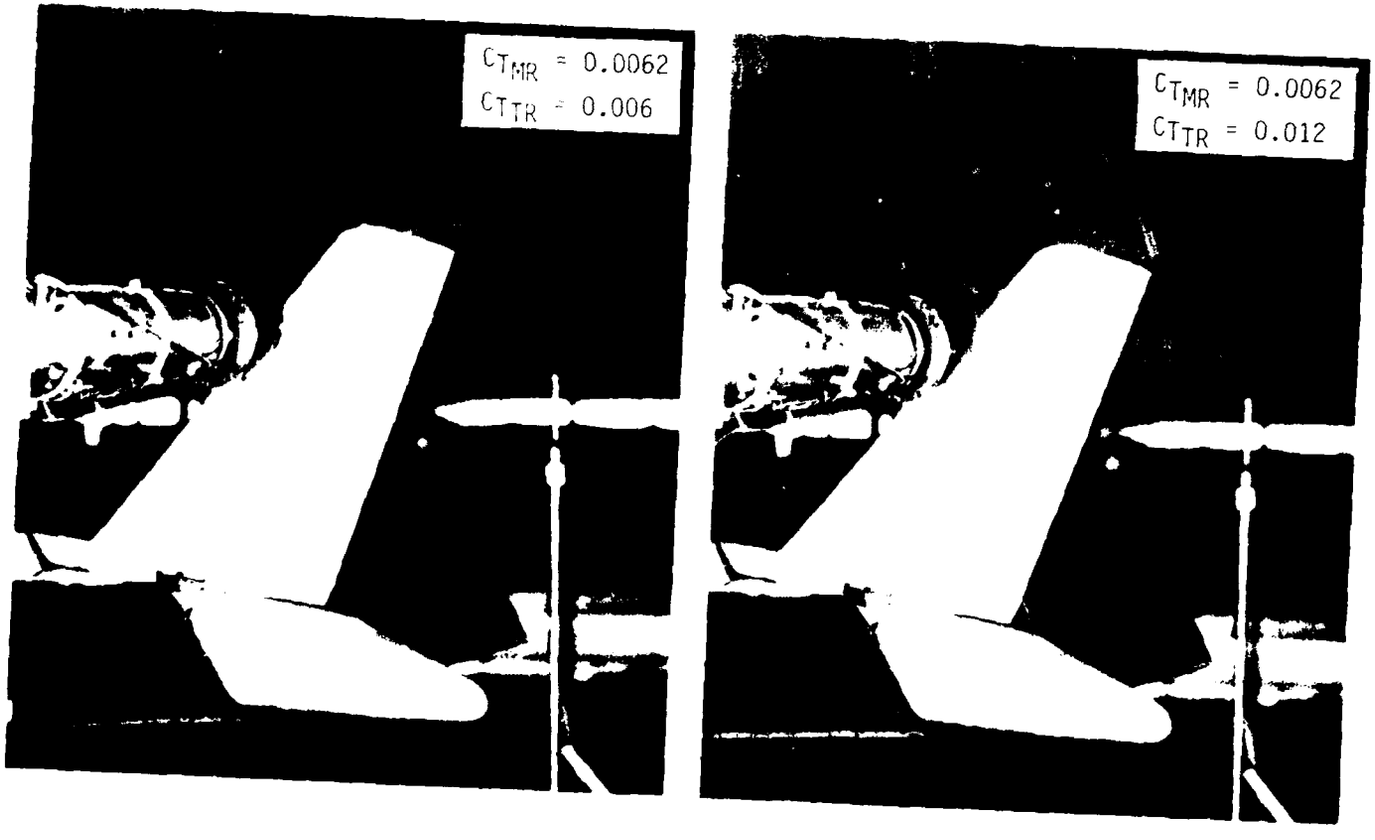

Figure 17. Effects of Rail Rotor Thrust on Fin Tuft Pattern in Left Sideslip Flight (ψ = 40°, V = 30 KTS)

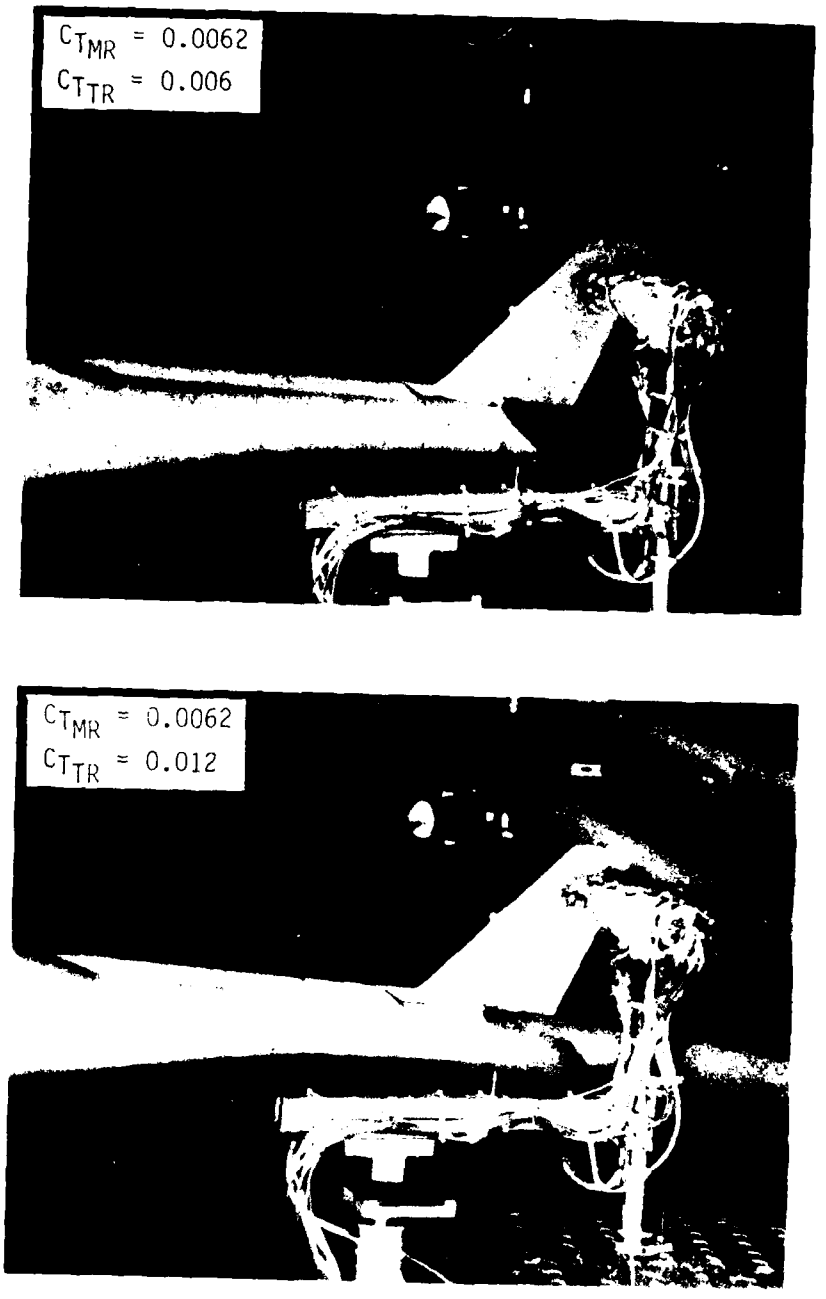

Figure 18. Effects of Tail Rotor Thrust on Fin Tuft Pattern Near Rearward Flight (ψ = 170°, V = 30 KTS)

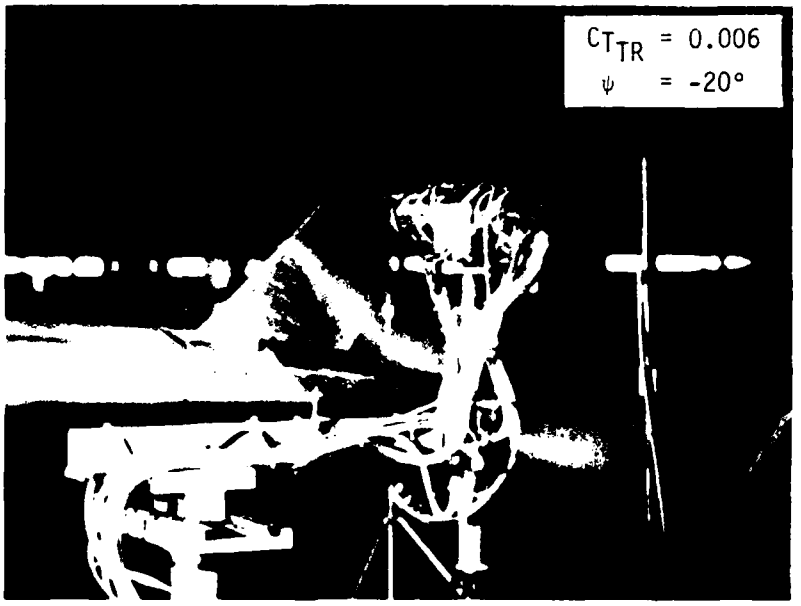

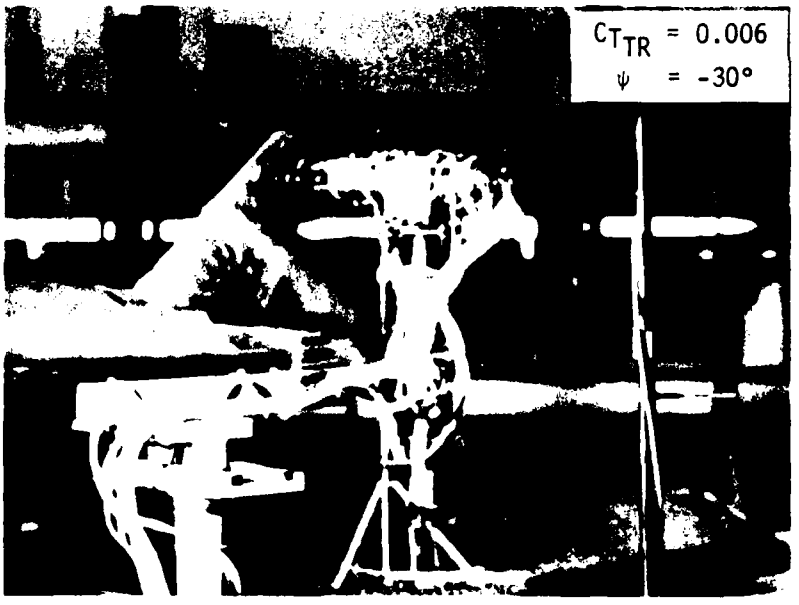

Figure 19. Fin Tuft Pattern in Right Sideward Flight ($C_{T_{MR}}$ = 0.0062, V = 30 KTS)

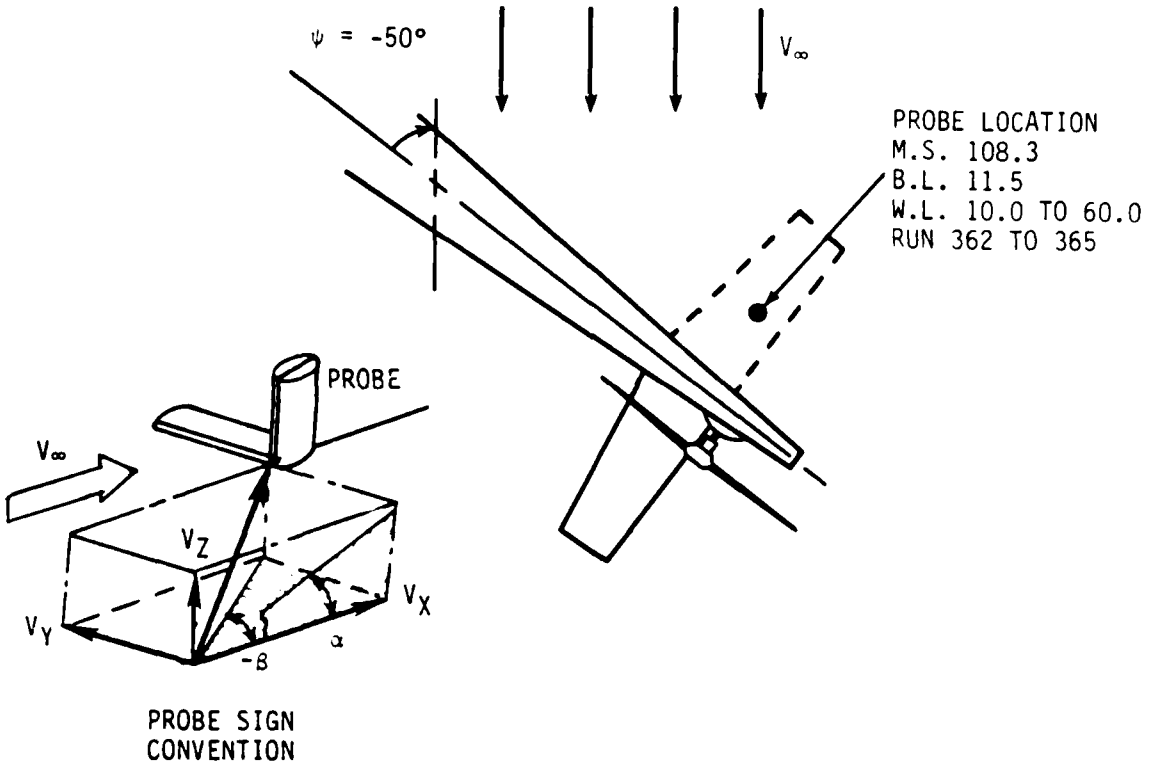

Figure 20. Top View of Hot Film Probe Location in a Right Sideslip (ψ = -50°)

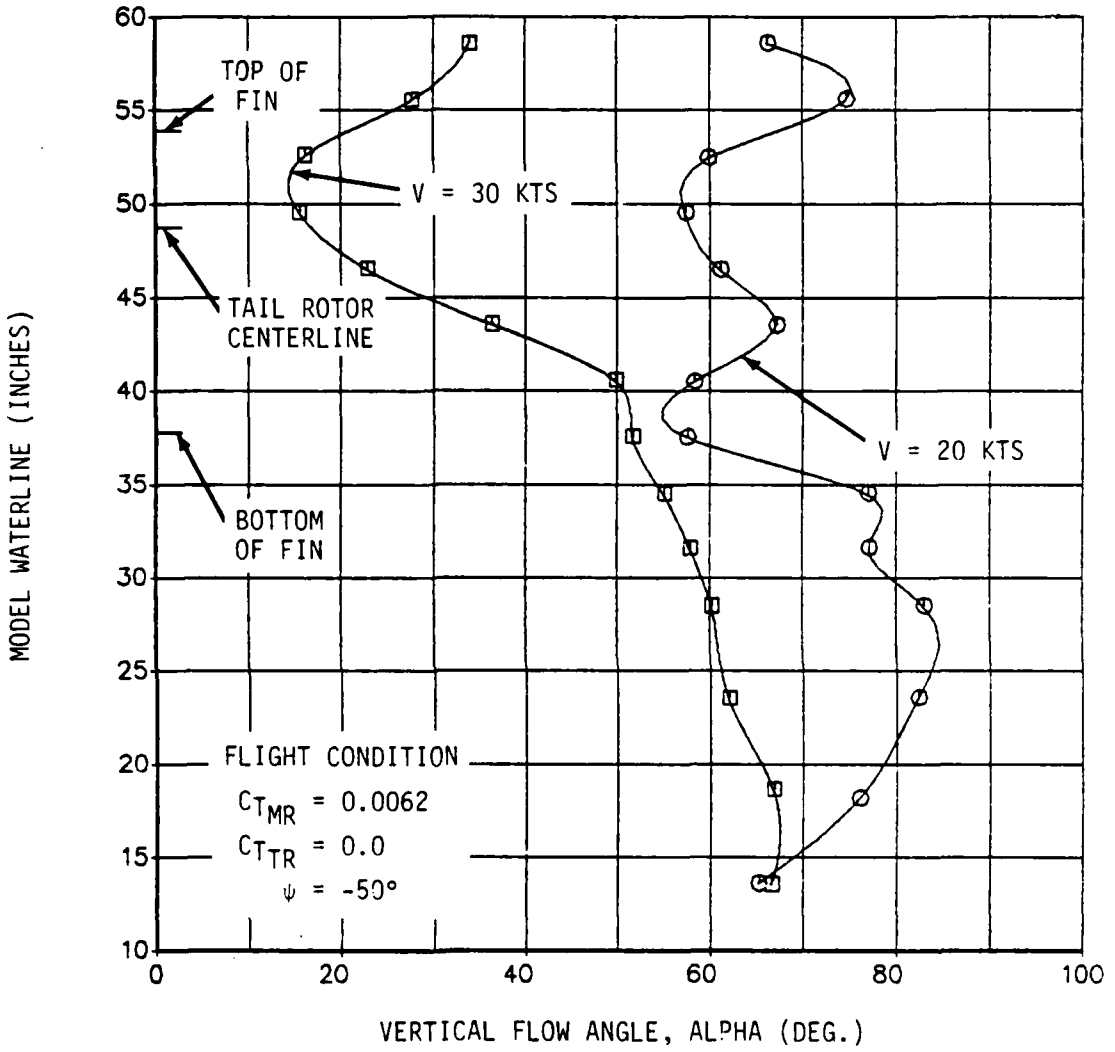

(a) Vertical Flow Component

Figure 21. Variation in the Vertical and Lateral Flow Components of the Main Rotor Wake Near the Empennage with Airspeed (Tail Rotor off, ψ = -50°)

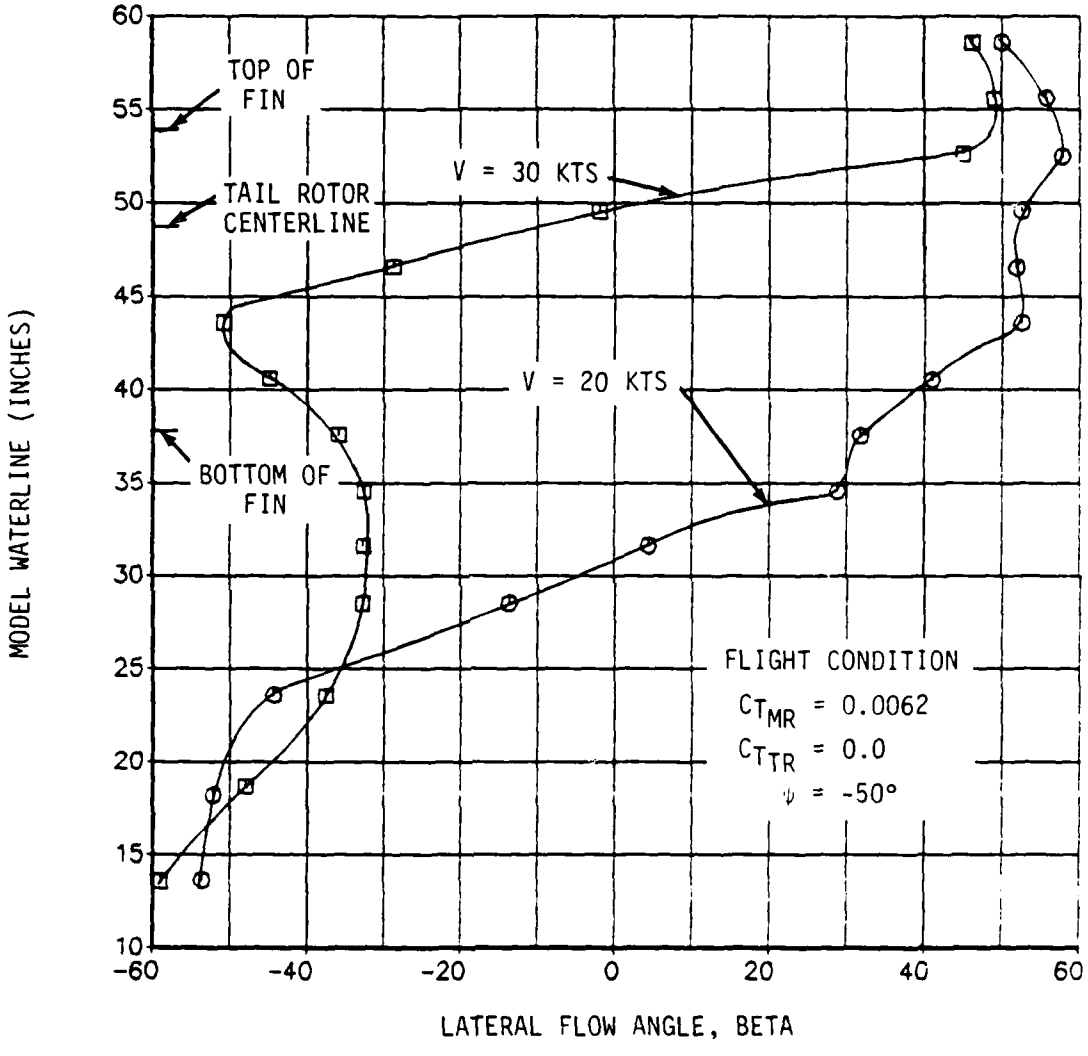

b. Lateral Flow Component

Figure 21. Continued.

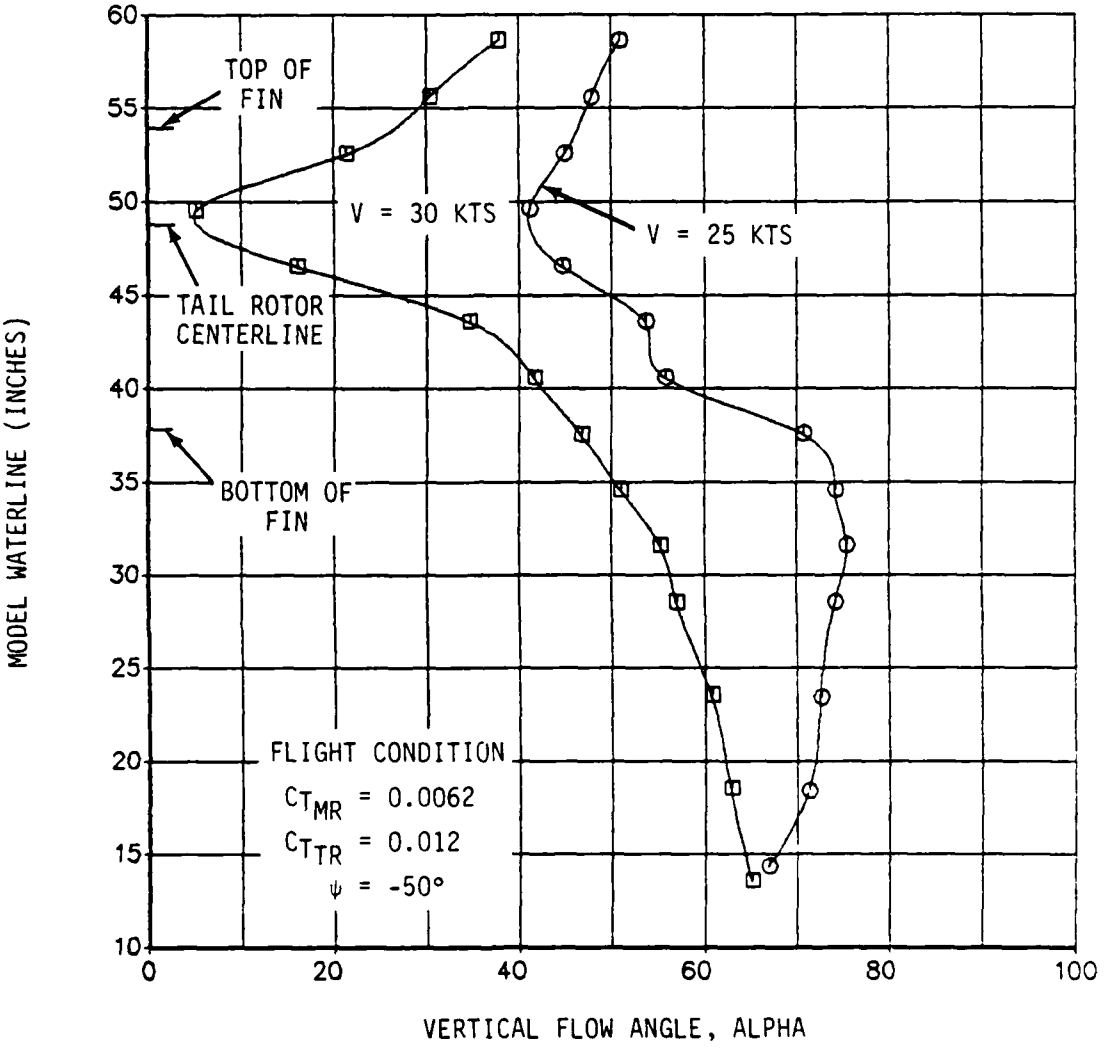

a. Vertical Flow Component

Figure 22. Variation in the Vertical and Lateral Flow Components of the Main Rotor Wake near the Empennage with Airspeed (Tail Rotor on, ψ = -50°)

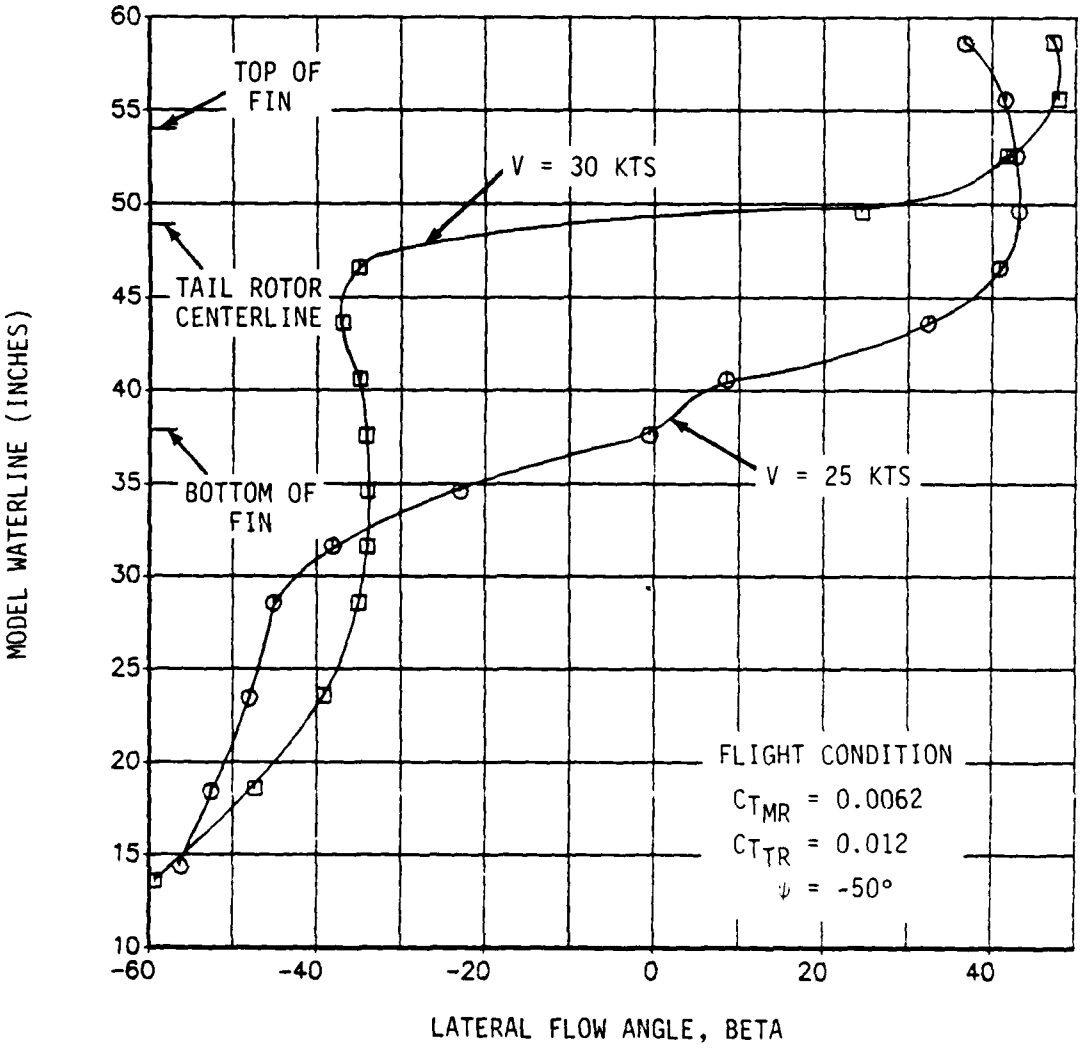

(b) Lateral Flow Component

Figure 22. Continued.

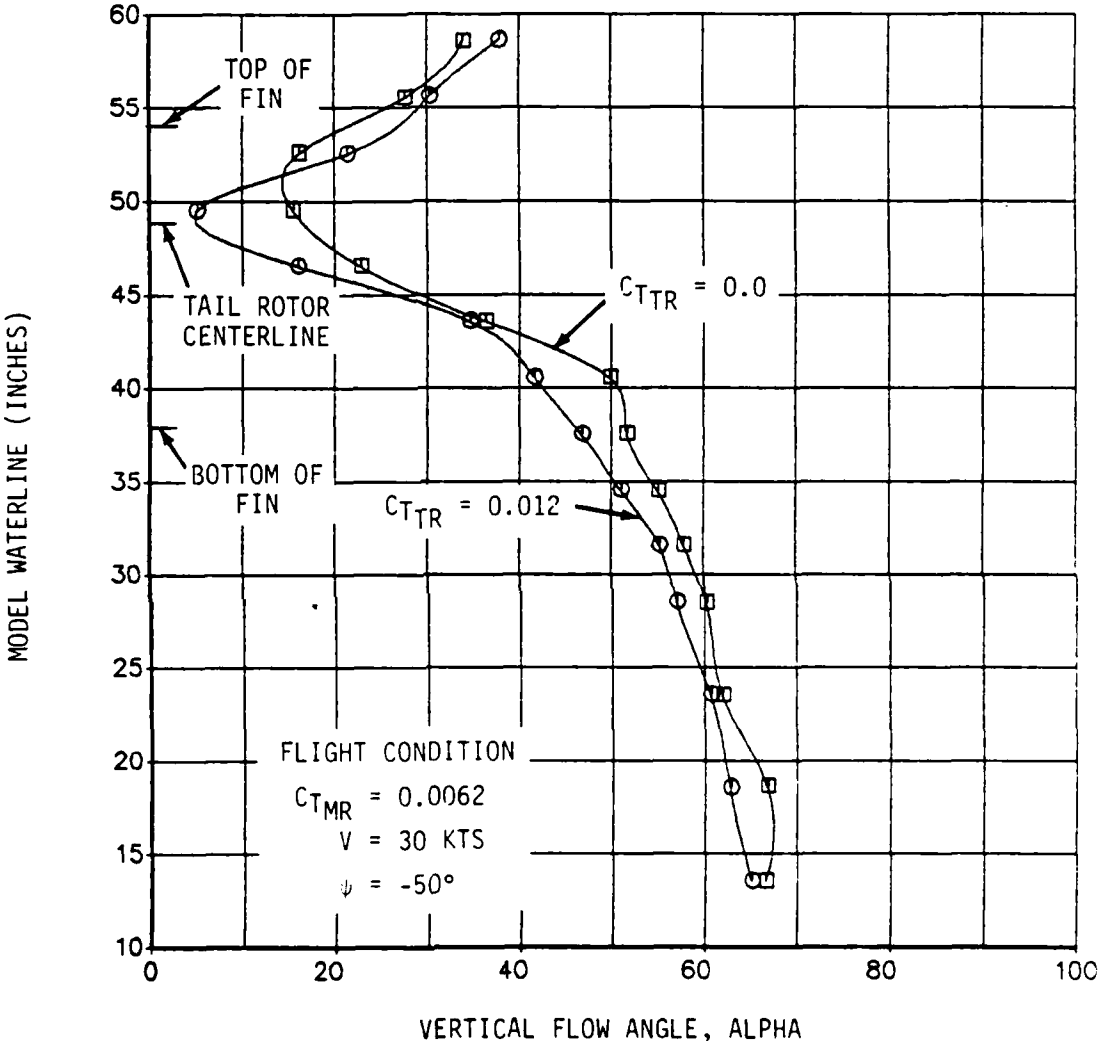

(a) Vertical Flow Component

Figure 23. Variation in the Vertical and Lateral Flow Components of the Main Rotor Wake Near the Empennage with Tail Rotor Thrust (V = 30 KTS, ψ = -50°)

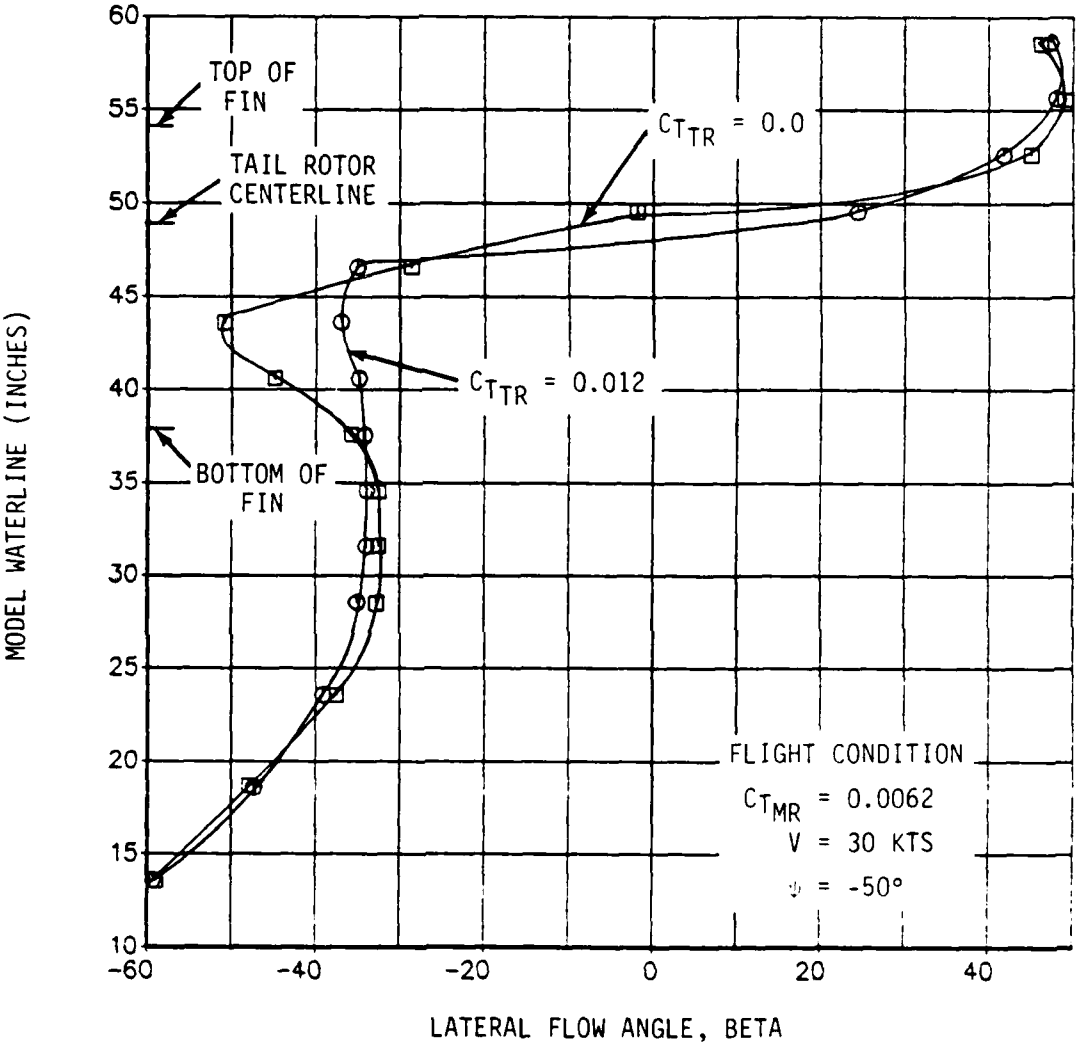

(b) Lateral Flow Component

Figure 23. Continued.

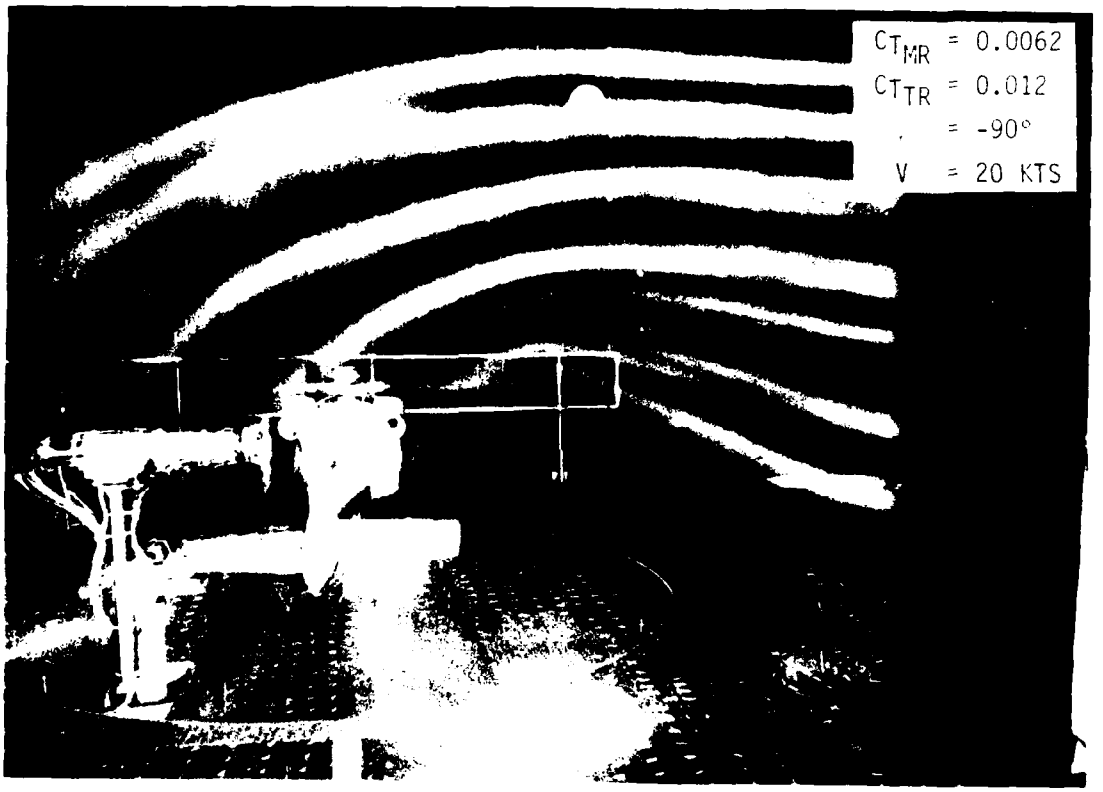

Figure 24. Ground Vortex Near the Empennage in Right Sideward Flight

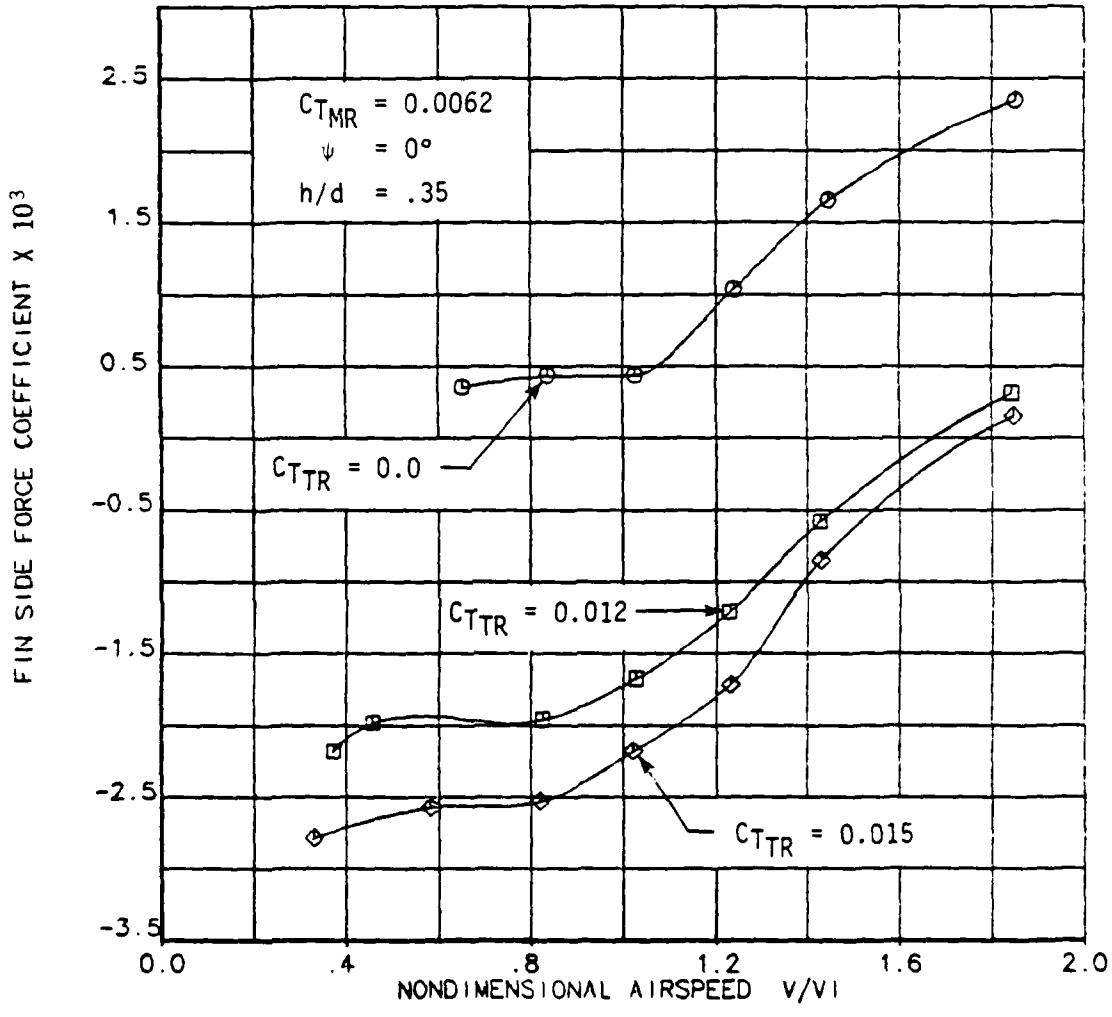

a. Forward Flight (ψ=0)

Figure 25. Effects of Airspeed on Fin Side Force Coefficient for Various Levels of Tail Rotor Thrust.

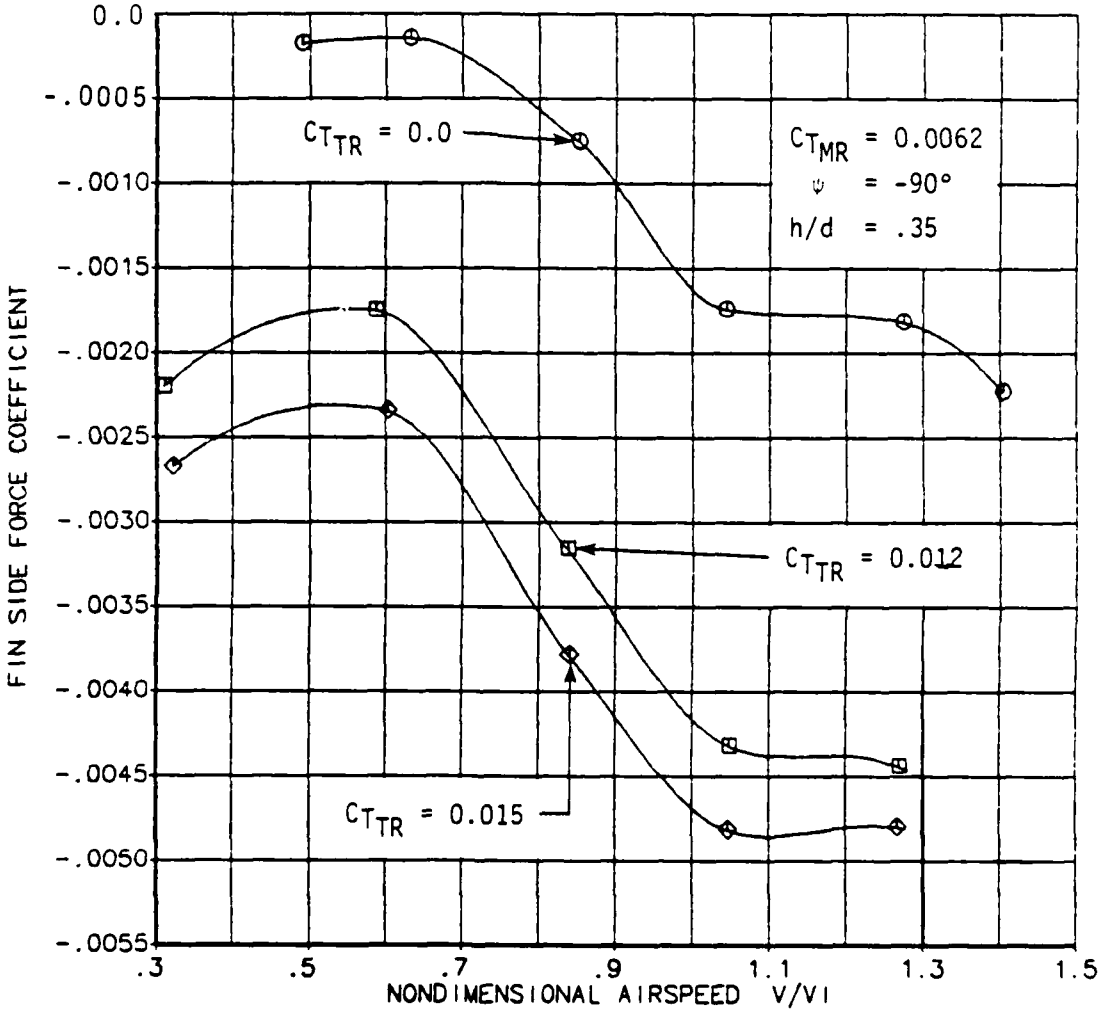

b. Right Sideward Flight (ψ=-90°)

Figure 25. Continued.

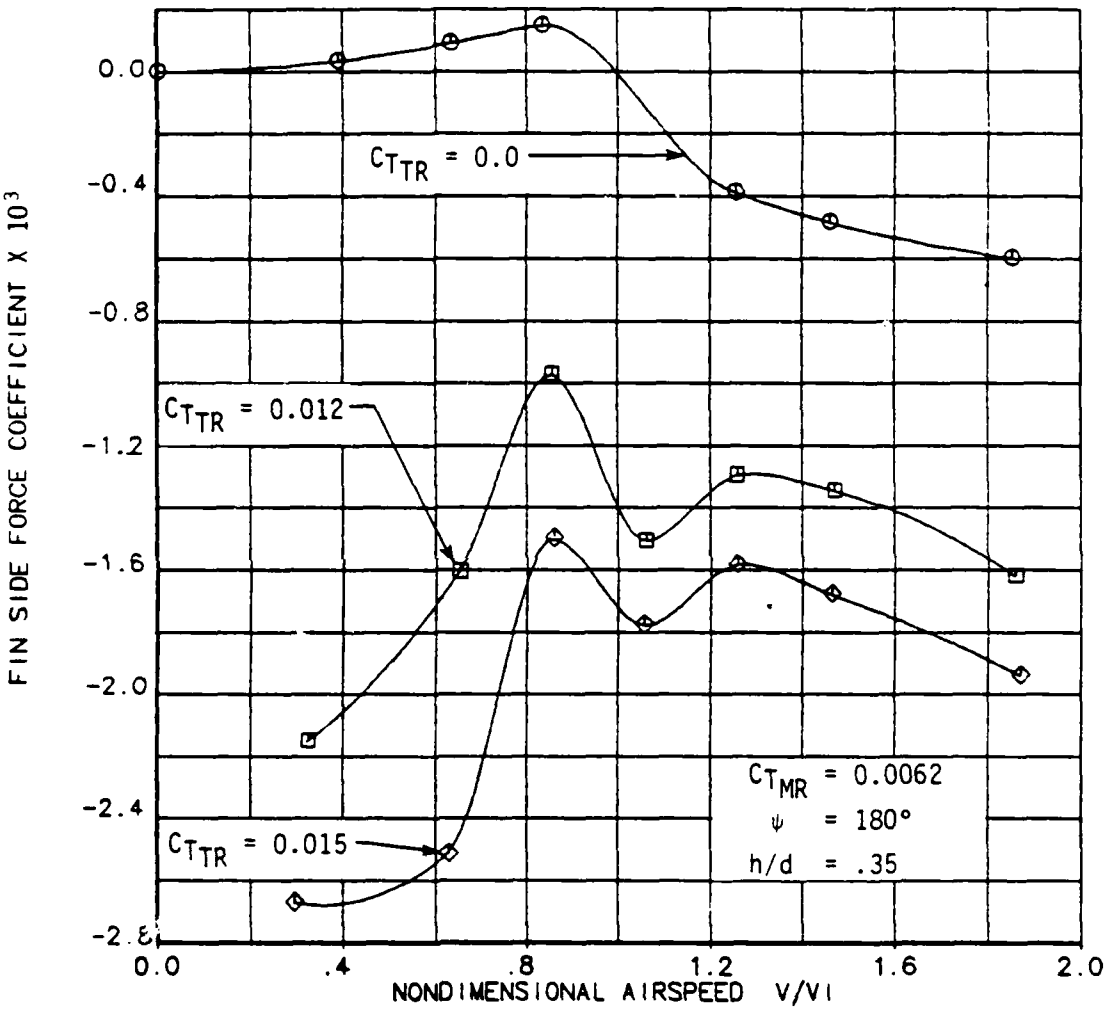

c. Rearward Flight (ψ=180°)

Figure 25. Continued.

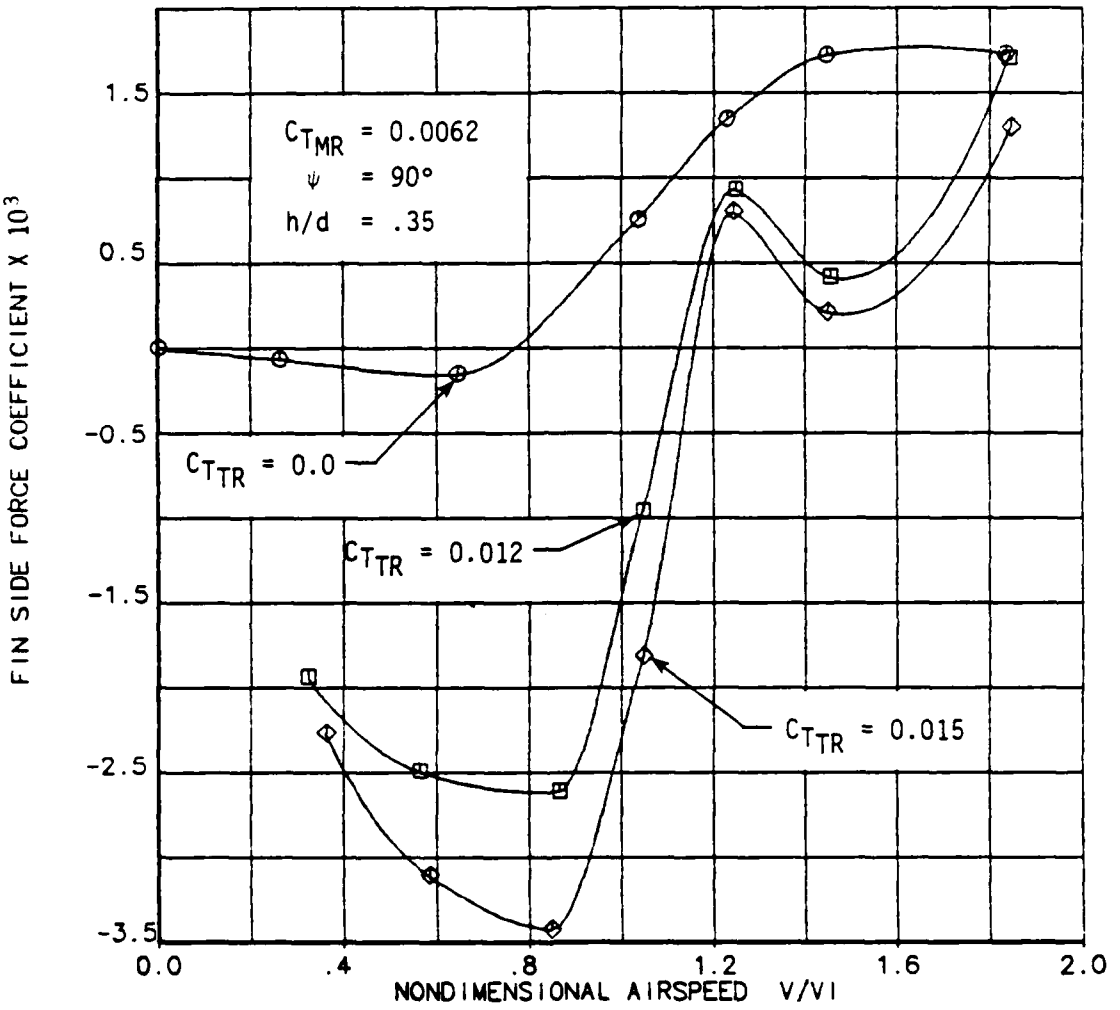

d. Left Sideward Flight (ψ=+90°)

Figure 25. Continued.

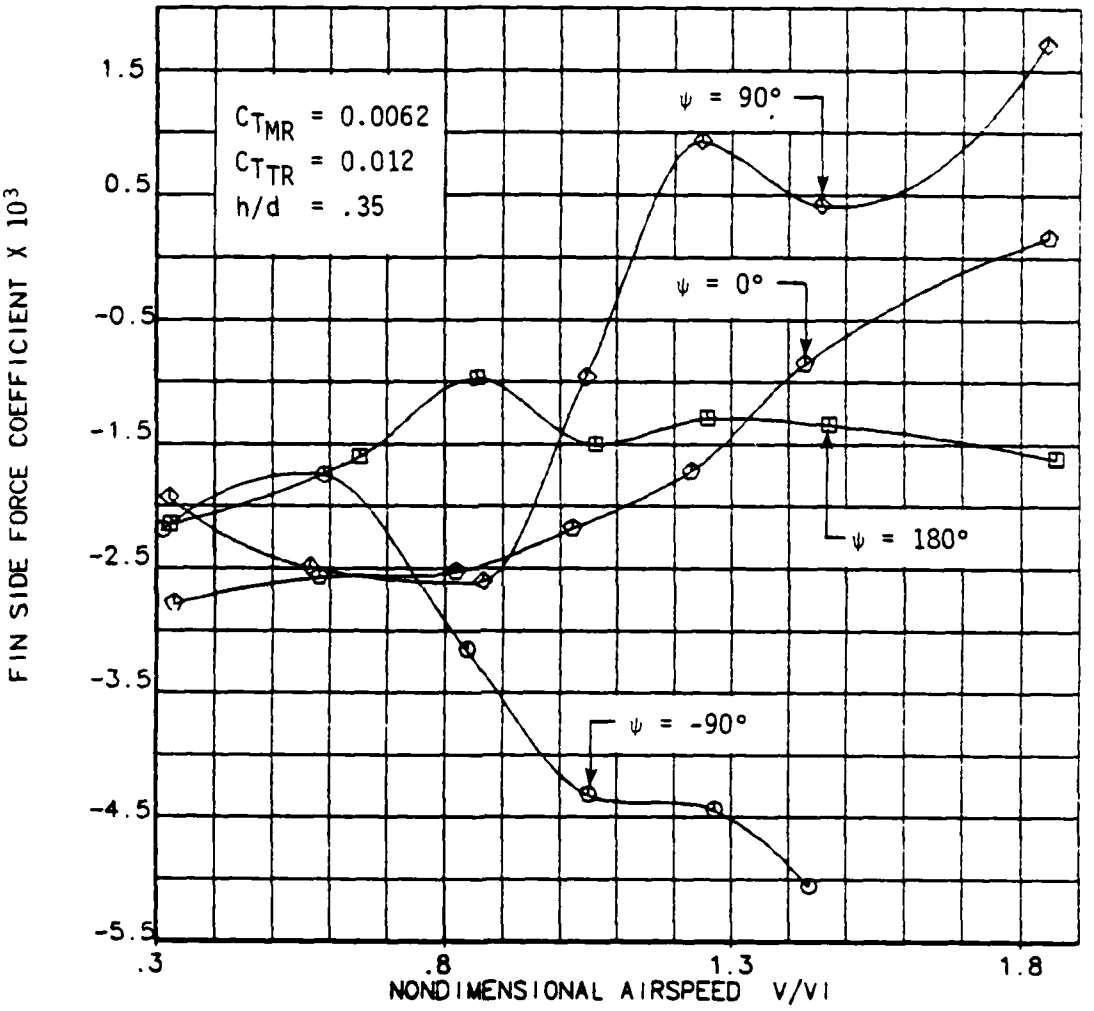

Figure 26. Comparison of Fin Side Force Variations Over the Transition Speed Regime for Different Wind Azimuths.

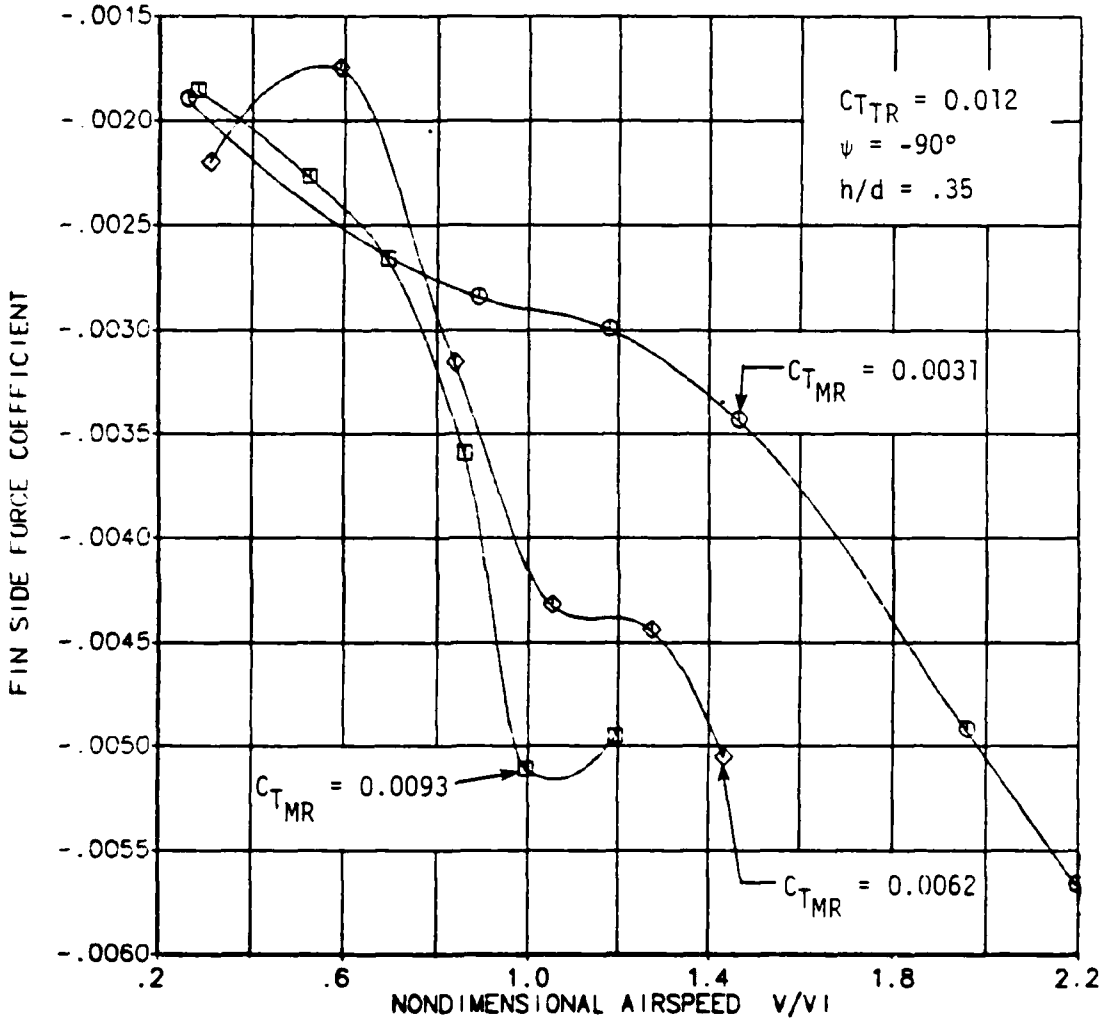

Figure 27. Effect of Main Rotor Thrust on Fin Side Force Coefficient in Right Sideward Flight.

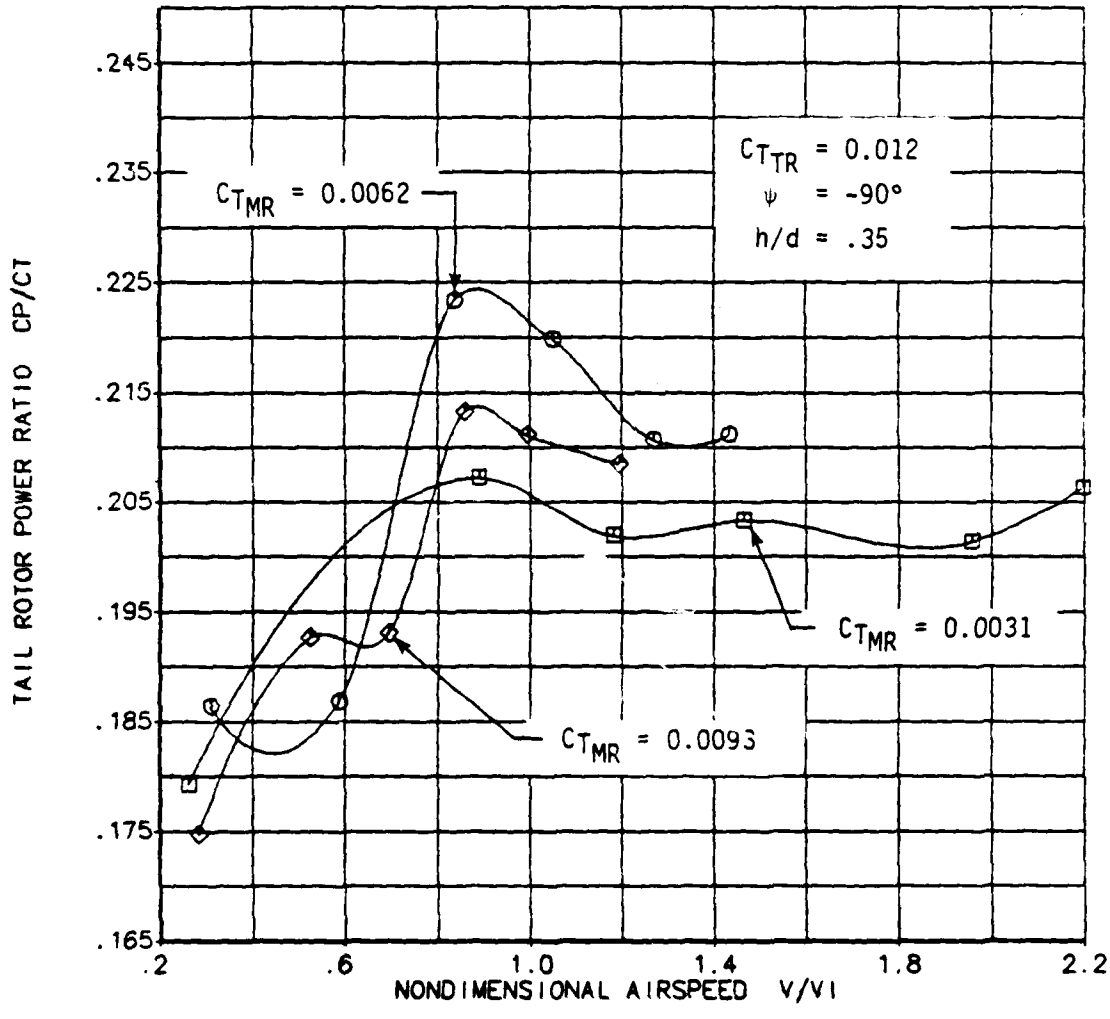

Figure 28. Effect of Main Rotor Thrust on Tail Rotor Power to Thrust Ratio in Right Sideward Flight.

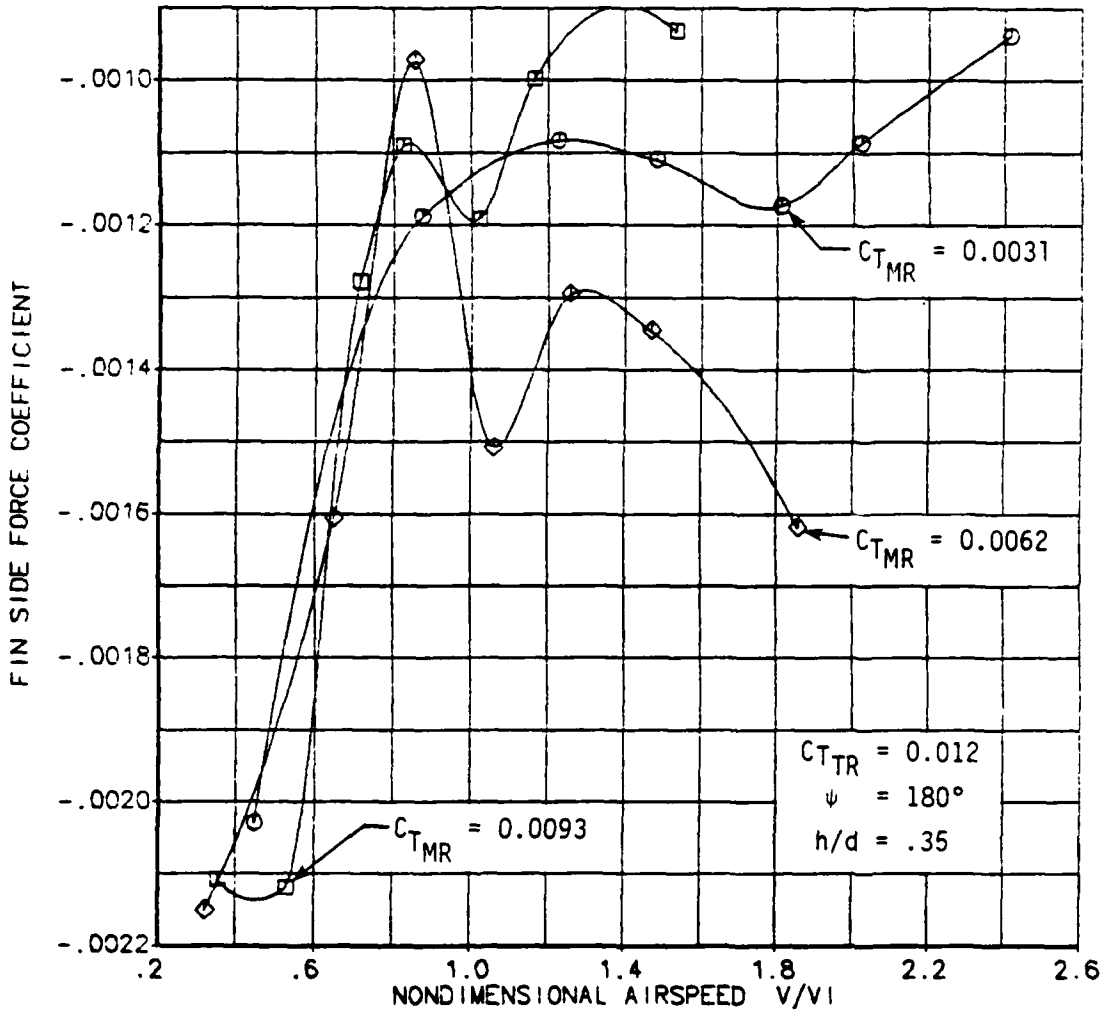

Figure 29. Effects of Main Rotor Thrust on Fin Side Force Coefficient in Rearward Flight.

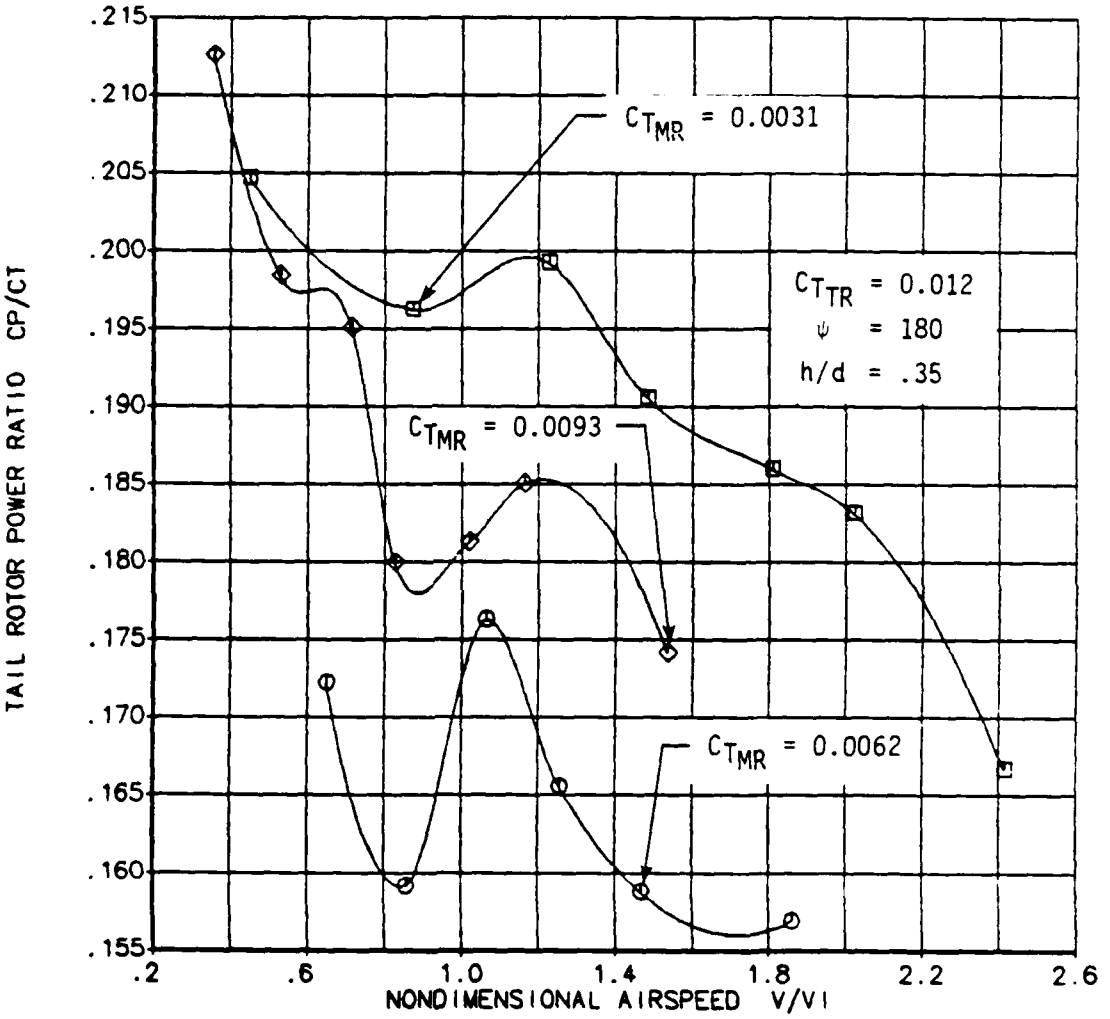

Figure 30. Effect of Main Rotor Thrust on Tail Rotor Power to Thrust Ratio in Rearward Flight.

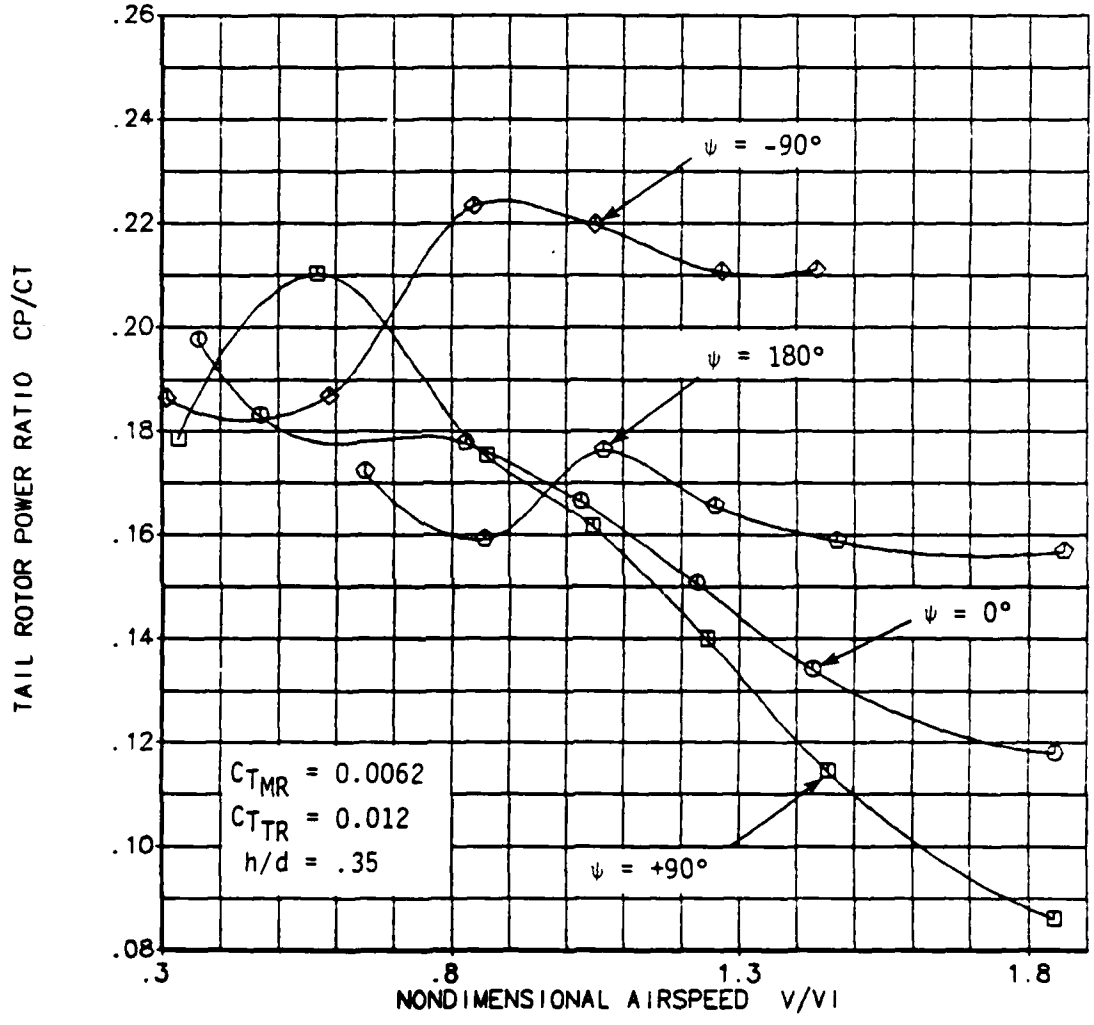

Figure 31. Comparison of Variations in Tail Rotor Power to Thrust Ratio Over the Transition Speed Regime for Different Wind Azimuths.

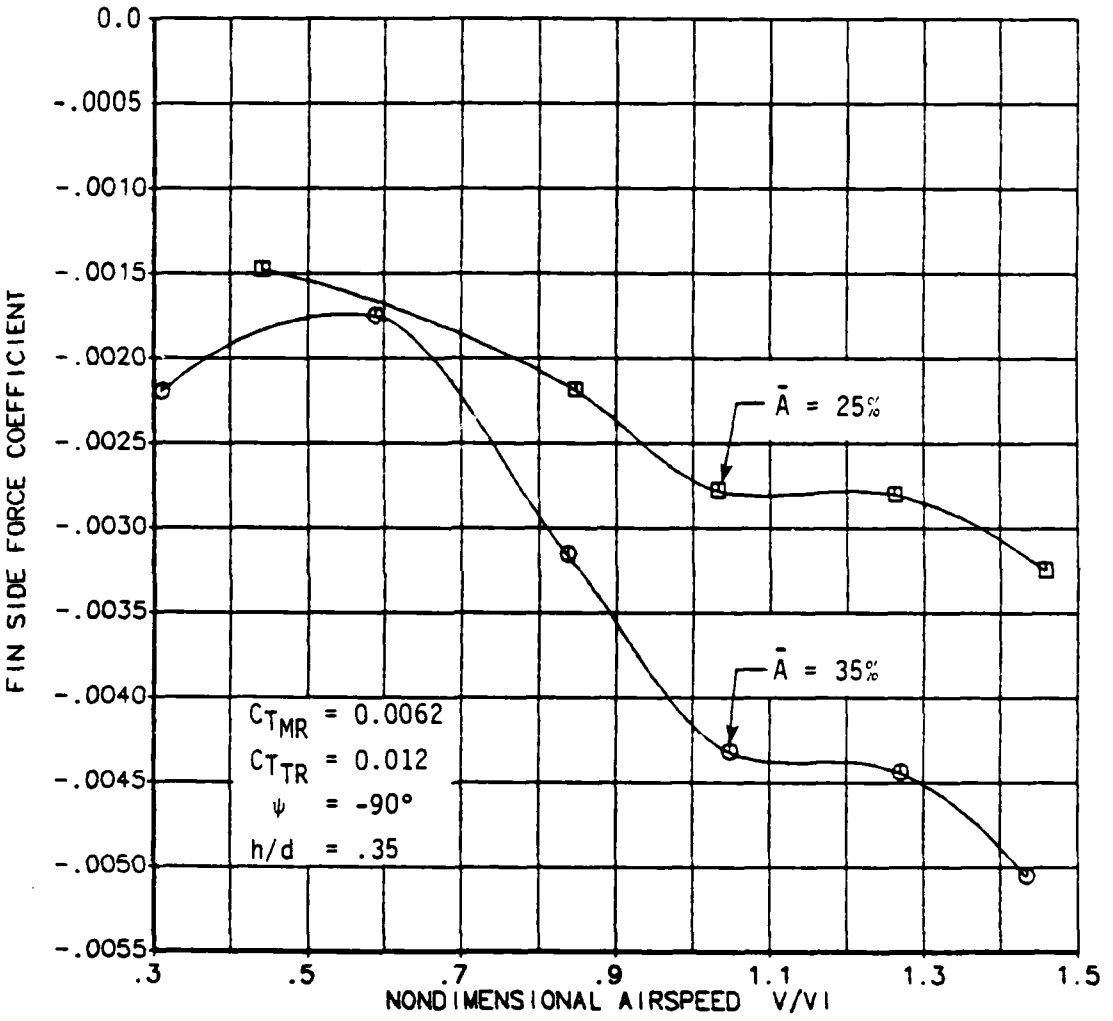

Figure 32. Variation in Fin Side Force Coefficient as a Function of Fin Size for Right Sideward Flight.

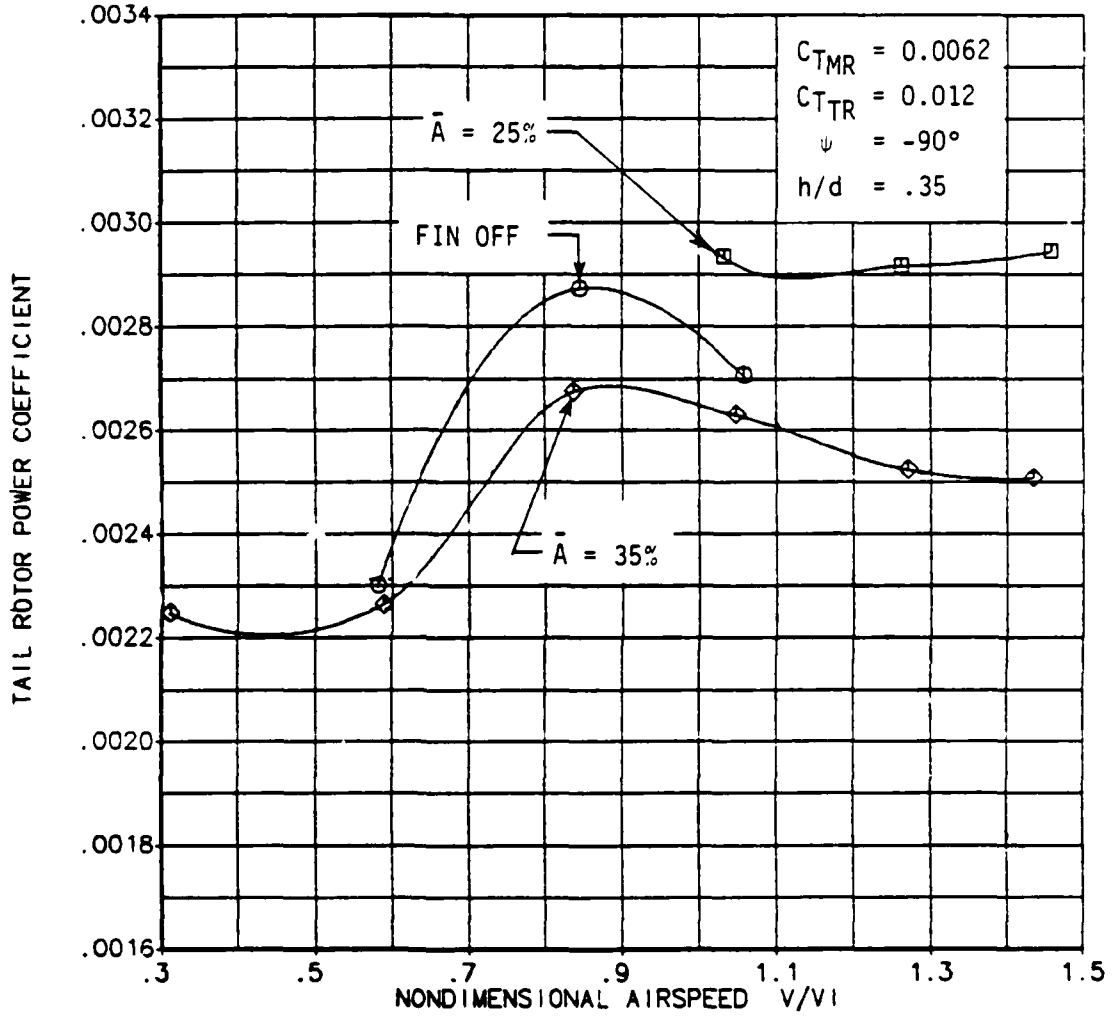

Figure 33. Variation in Tail Rotor Power Coefficient as a Function of Fin Configuration for Right Sideward Flight.

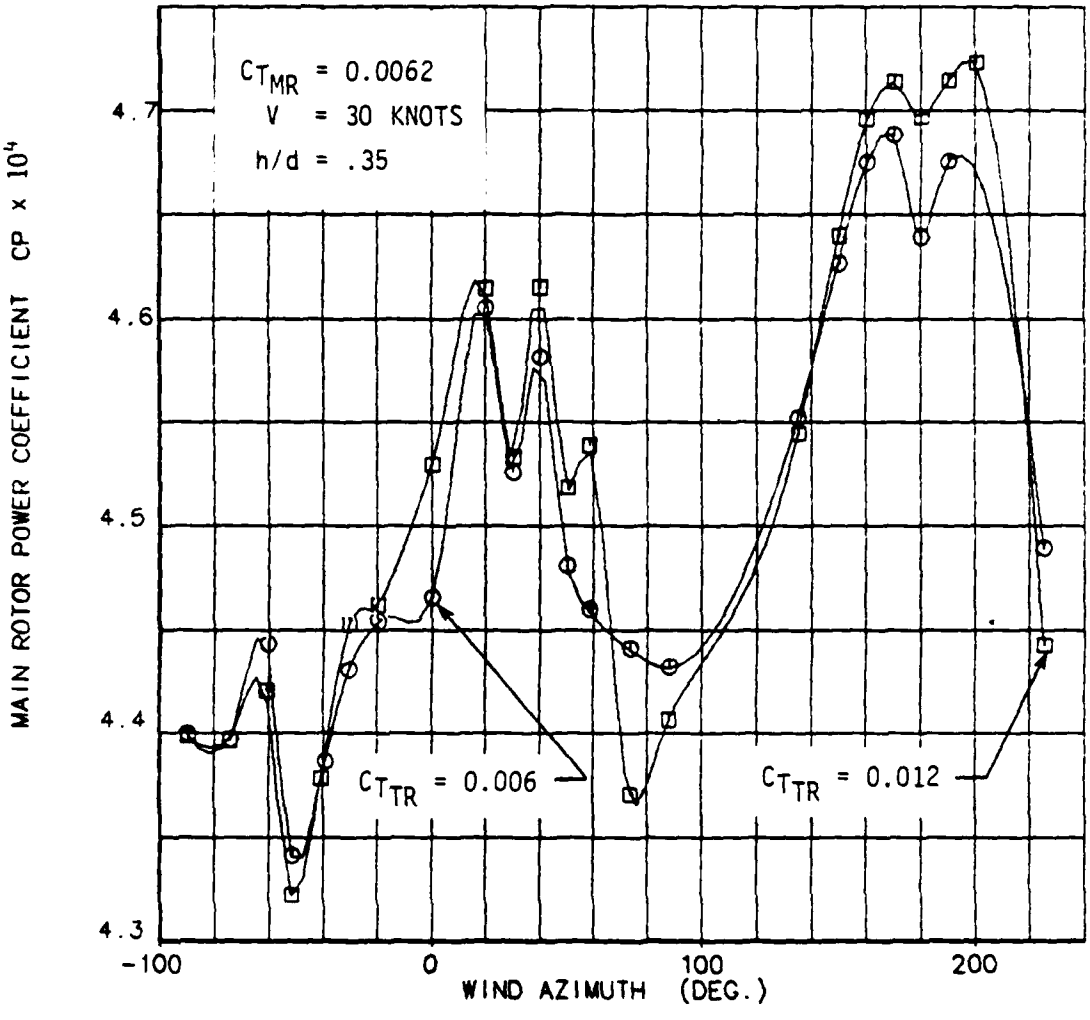

Figure 34. Variation of Main Rotor Power Coefficient at a Fixed Thrust Condition as a Function of Wind Azimuth and Tail Rotor Thrust.

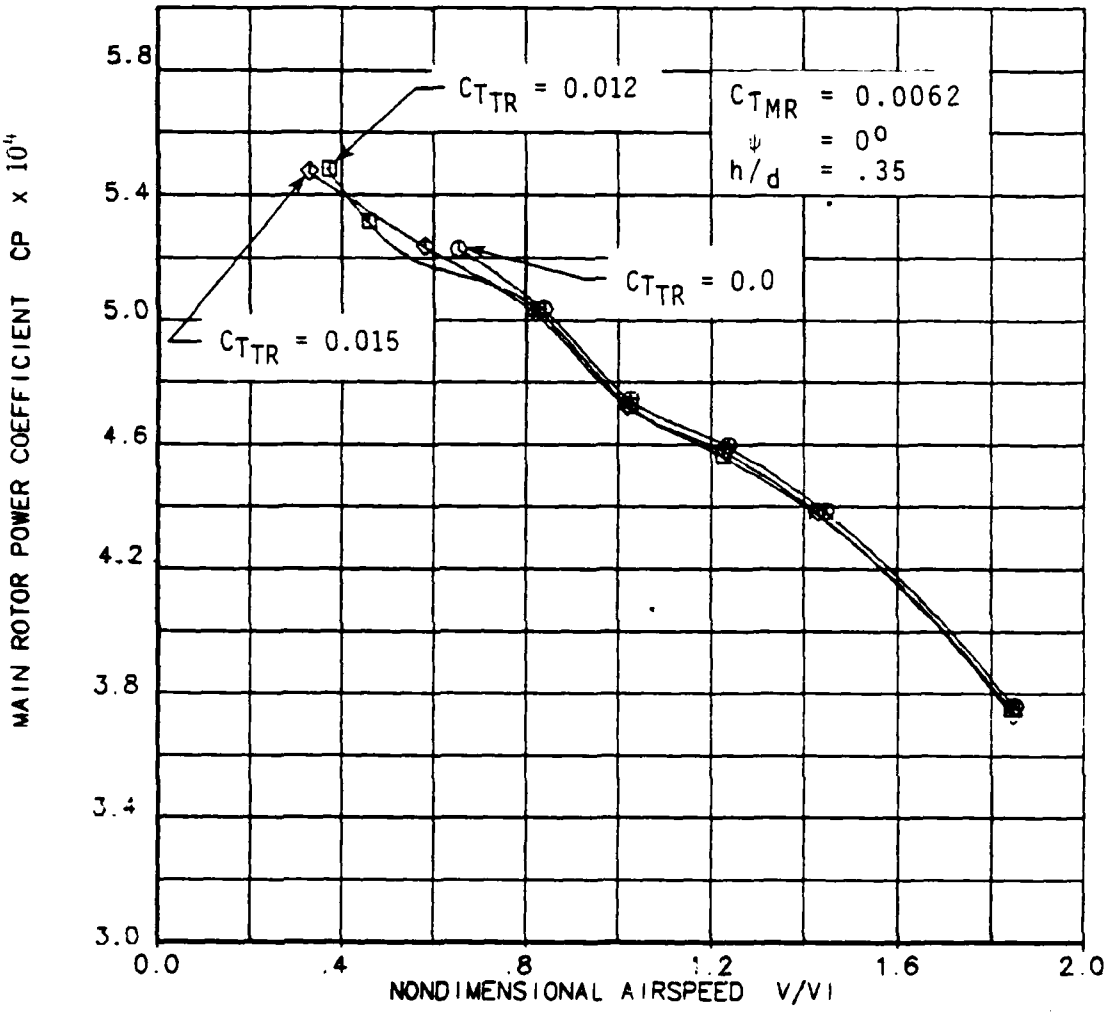

a. Forward Flight (ψ=0)

Figure 35. Effects of Tail Rotor Thrust Level on Main Rotor Power Coefficient Over the Transition Speed Regime.

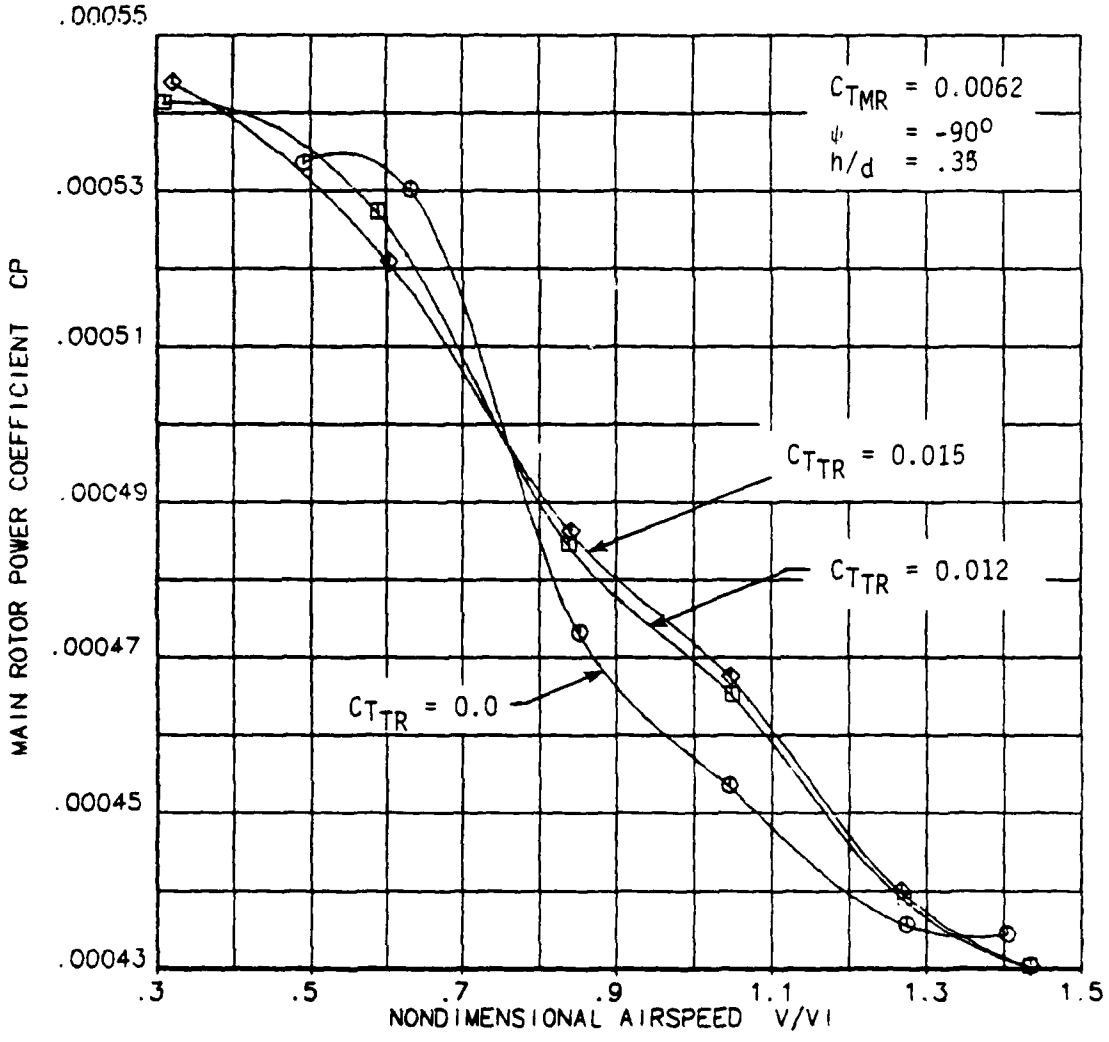

b. Right Sideward Flight (ψ=-90°)

Figure 35. Continued

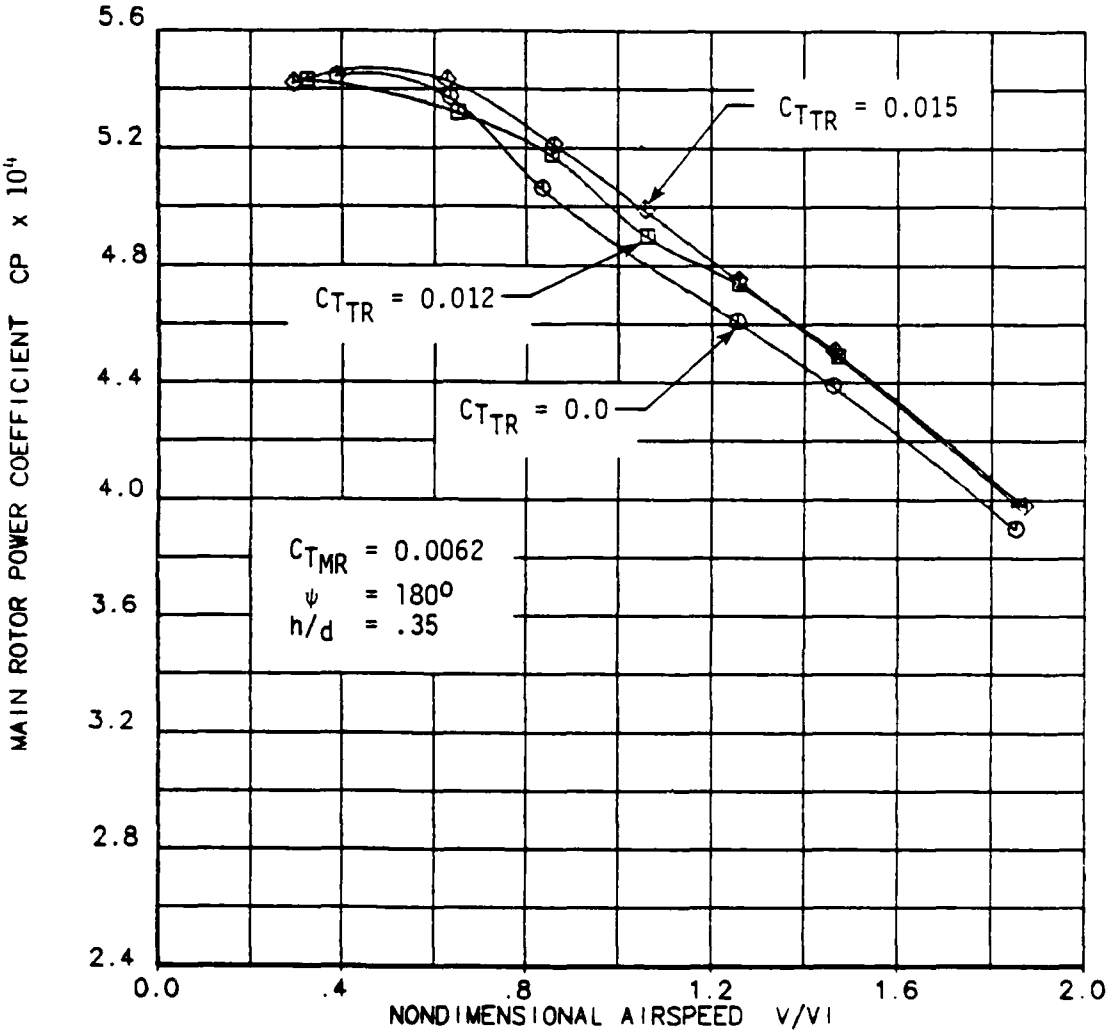

c. Rearward Flight (ψ=180°)

Figure 35. Continued.

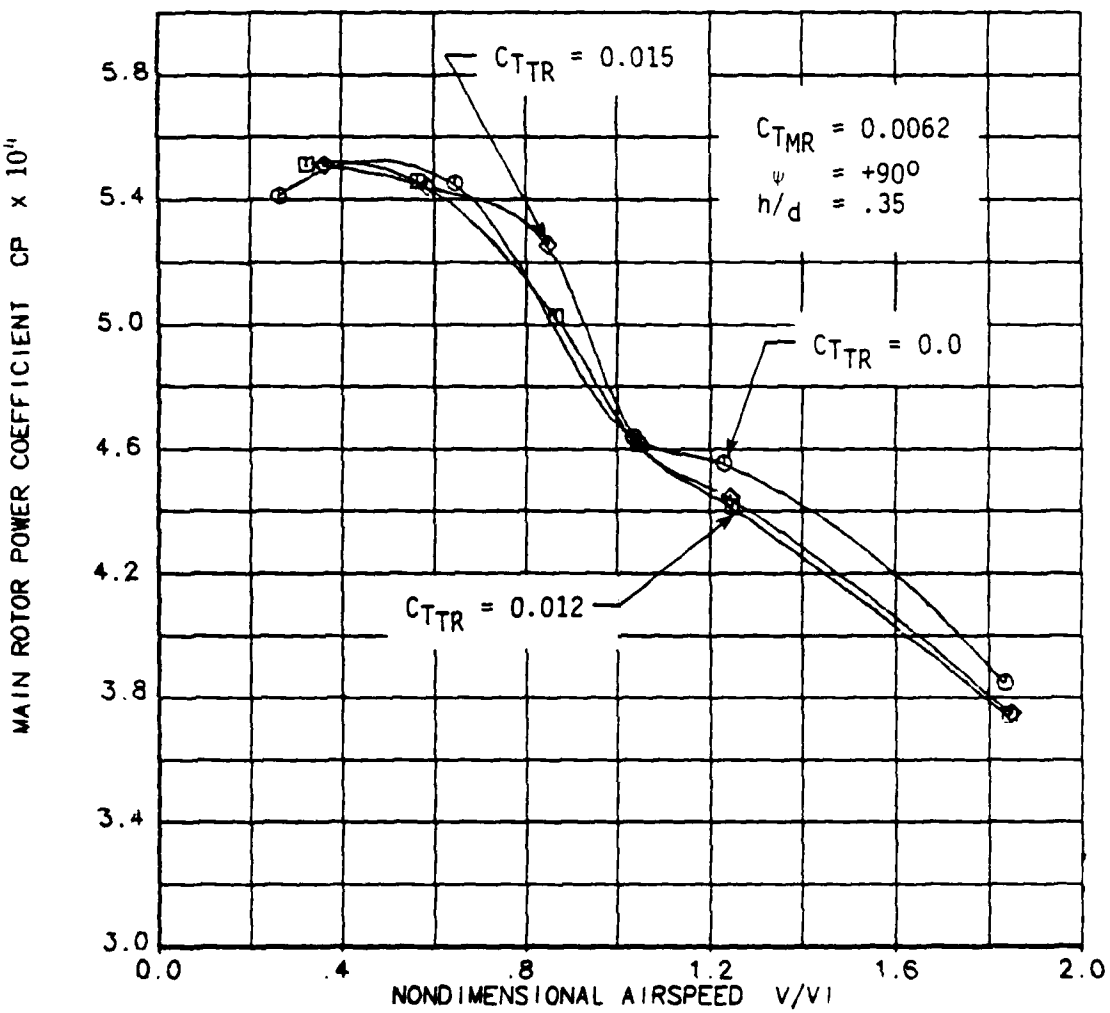

d. Left Sideward Flight (ψ=+90°)

Figure 35. Continued.

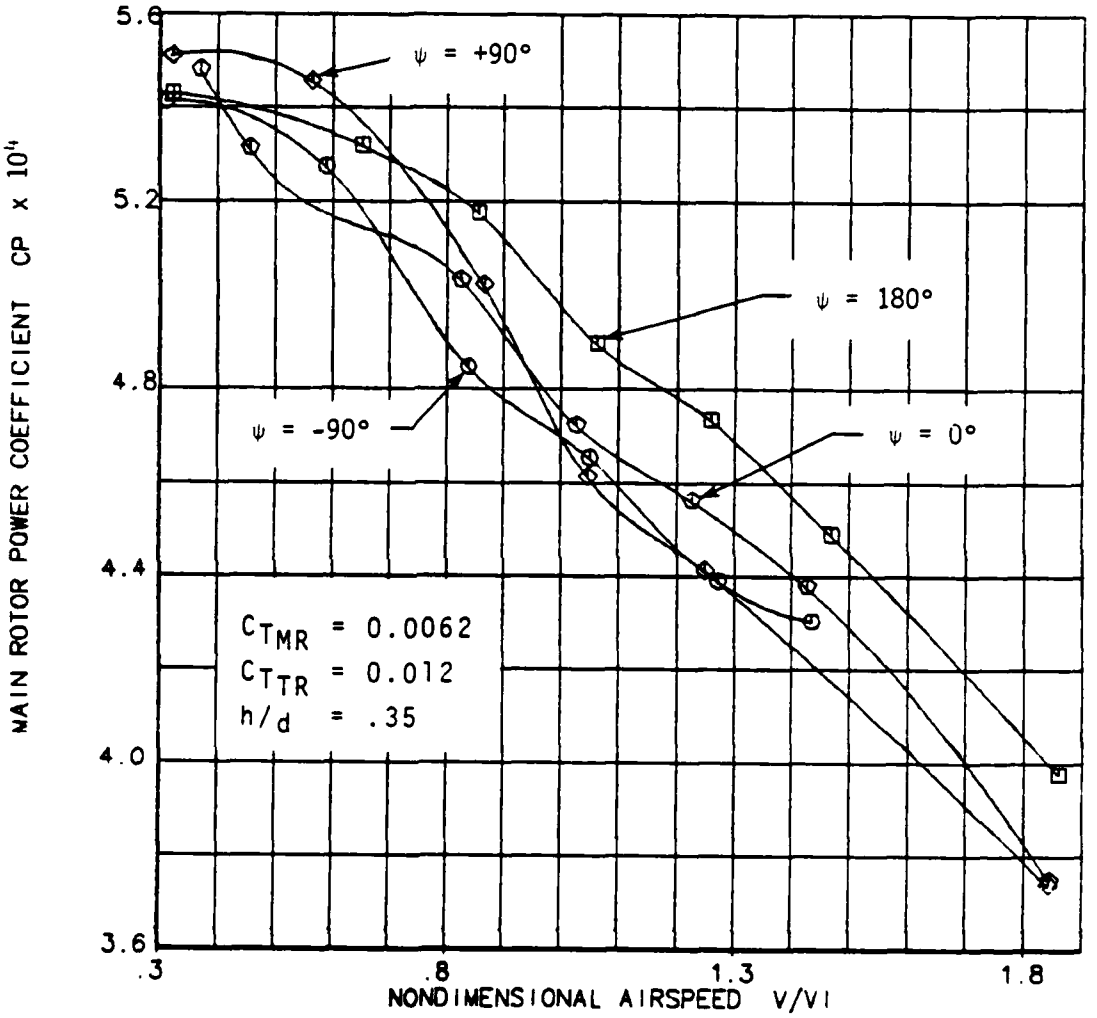

Figure 36. Comparison of Variations in Main Rotor Power Coefficient over the Transition Speed Regime for Different Wind Azimuths.

CONCLUSION

A wind tunnel investigation of aerodynamic interactions of the tail rotor and fin under the influence of the main rotor wake was conducted at the Boeing Vertol V/STOL wind tunnel. Data were obtained for a wide range of test conditions. The effects of varying main rotor, and tail rotor thrust were studied as well as the influence of free stream airspeed and azimuth. The following conclusions have been reached:

- The main rotor wake induces a substantial sideward flow component at the empennage as evidenced by the large negative fin incidence angles required for zero sideforce.

- Variations in fin sideforce with changes in wind direction show that a maximum adverse fin load can occur at a wind azimuth less than right sideward flight (ψ = -90°) due to interaction with the main rotor tip vortices.

- Tail rotor power variations (at a constant thrust condition) for changes in wind azimuth indicate that the fin can shield the tail rotor from flow anomalies such as the main rotor tip vortex.

- The passage of the ground vortex in proximity to the empennage has a significant effect on fin and tail rotor loads. The effects of the ground vortex extend out to wind azimuths of ±90 degrees. The interaction increases significantly as main rotor disk loading increases. However, the maximum influence of the ground vortex occurred at similar values of nondimensional airspeed for different levels of main rotor thrust.

- Tail rotor pressurization of the vertical fin is the primary source of adverse fin side force. Increases in tail rotor thrust also increase fin loads. In addition, adverse fin loads grow as the blockage ratio increases. The trend toward larger fins for improved directional control characteristics for the tail rotor inoperative condition will produce larger adverse loads as the susceptibility of the vertical fin to aerodynamic interactions increases.

- The interaction between the tail rotor and fin is also affected by the fin shape. Tail rotor power required for the 25% blocakge fin was higher than that measured for the fin off case. Further research is required to substantiate the effects of fin shape on tail rotor/fin interactions.

REFERENCES

1. Hanker, E.J.,Jr., Smith, R.P., "Parameters Affecting Helicopter Interactional Aerodynamics In Ground Effect," AHS Preprint No. A-83-39-57-4000, presented at the 39th Annual Forum of the American Helicopter Society, St. Louis, MO, May 1983.

2. Wiesner, W., and Kohler, Gary, "Tail Rotor Design Guide," Boeing Vertol Company; USAAMRDL Technical Report 73-99, Eustis Directorate, U.S. Army Air Mobility Research and Development Laboratory, Fort Eustis, Virginia, January 1974. AD775391.

3. Yeager, William T., Jr., Young, Warren H., Jr., and Mantay, Wayne R., "A Wind Tunnel Investigation of Parameters Affecting Helicopter Directional Control at Low Speeds in Ground Effect," NASA Technical Note D-7694, Langley Directorate, U.S. Army Air Mobility Research and Development Laboratory, Langely Research Center, Hampton, Virginia, November 1974.

4. Huston, Robert J., and Morris, Charles E. K., Jr., "A Wind Tunnel Investigation of Helicopter Directional Control in Rearward Flight in Ground Effect," NASA Technical Note D-6118, National Aeronautics and Space Administration, Langley Research Center, Hampton, Virginia, March 1971.

5. Curtiss, H.C., Jr., Sun, M., Futman, W.F., and Hanker, E.J., Jr., "Rotor Aerodynamics in Ground Effect at Low Advance Ratios," AHS Preprint No. 81-5, presented at the 37th Annual Forum of the American Helicopter Society, New Orleans, LA, May 1981.

6. Sheridan, P.F., and Smith, R.P., "Interactional Aerodynamics - A New Challenge to Helicopter Technology," Preprint No. 79-59, presented at the 35th Annual National Forum of the American Helicopter Society, Washington, D.C., May 1979.

7. Sheridan, P.F., and Wiesner, W., "Aerodynamics of Helicopter Flight Near the Ground," Preprint No. 77.33-04, presented at the 33rd Annual Forum of the American Helicopter Society, Washington, D.C., May 1977.

PUBLICATION

The results of this research were published in a paper entitled "Parameters Affecting Helicopter Interactional Aerodynamics in Ground Effect" which was presented at the 39th Annual Forum of the American Helicopter Society, May 1983 (AHS Preprint A-83-39-57-4000). This paper includes the results of the closely related contract entitled "Investigation of Operational and Design Factors Resulting from Main Rotor and Tail Rotor Interactions," that was funded, under contract, by the Applied Technology Laboratory, Ft. Eustis. Mr. Robert P. Smith is the Technical Monitor for the Eustis Contract.

PERSONNEL

Shortly after the completion of the wind tunnel test Phil Sheridan, the principal investigator, suddenly passed away. The responsibilities of principal investigator were bestowed upon Dr. John Shaw, an Engineering Specialist in the Flying Qualities group at Boeing Vertol. In June of 1982 Dr. Shaw was promoted to Technology Manager of a new aircraft design program. At that time, Mr. Edward Hanker, Jr. was assigned as the Principal Investigator of the contract. The time periods of each individuals service as the principal investigator are listed below.

17 July 1978 to August 1981	Mr. Philip P. Sheridan
August 1981 to 1 June 1982	Dr. John Shaw
1 June 1982 to 1 April 1983	Mr. Edward J. Hanker, Jr.

Mrs. Jesse Achey, a senior technician on the Wind Tunnel Staff, and Mr. Carl Robinson, an engineer in the Flying Qualities Staff, were also supported part time by this research program.

No advanced degrees were earned by the individuals employed by this program.

END

DATE
FILMED

9 — 83

DTIC